Geometry of folded and boudinaged pegmatite veins emplaced within a strike-slip shear zone: A case study from the Caledonian orogen, northern Scotland.

Alsop, G.I.1, Strachan, R.A.2, Holdsworth, R.E.3, & Burns, I.M.4

1. Department of Geology and Geophysics, University of Aberdeen, Aberdeen, AB24 3UE, UK.
2. School of the Environment, Geography and Geosciences, University of Portsmouth, Burnaby Rd., PO1 3QL, UK.
3. Department of Earth Sciences, South Rd, University of Durham, Durham, DH1 3LE, UK.
4. 6 Mackenzie Crescent, Bettyhill, By Thurso, Sutherland, Scotland.

Abstract

The deformation of sheet-like igneous intrusions in multiple orientations can give detailed insights into the kinematics of ductile flow in shear zones. Using the Torrisdale Vein Complex in the northern Scottish Caledonides as a case study, we examine the relationships between folded and boudinaged pegmatitic intrusions deformed by strike-slip dominated shear. Within the shear zone, intrusions that trend clockwise of the adjacent regional foliation were commonly (75%) folded, whereas >80% of pegmatites at anticlockwise angles were asymmetrically boudinaged, giving dextral senses of shear parallel to the dominant and gently-plunging mineral lineations. Pegmatite fold trains at high angles to foliation (Sn) display the greatest % shortening, marked by steeply plunging 'Z' shaped folds when viewed down plunge. Pegmatites typically form Class 1C folds and were therefore more competent than their host gneisses at the time of deformation, i.e. they were not in the magmatic state. Such fold geometries are consistent with flattened parallel folds and suggest that up to 0.5 homogenous flattening was superimposed on the folds. Fold styles also indicate viscosity contrasts between the pegmatites and host gneisses of between 50 and 250 at the time of folding. Fold hinges are dispersed about an arc within the steeply-dipping foliation, suggesting a component of hinge rotation towards the mineral lineation during non-coaxial deformation. Folded pegmatites may also display boudinage on their limbs indicating that fold limbs had rotated into the extensional field during progressive deformation. Pegmatite boudin trains are typically developed <45° anticlockwise of Sn and display the greatest % extension when trending sub-parallel to the shear zone foliation. Within such trains, individual shearband boudins are more anticlockwise than the overall train and show right-stepping relative to neighbouring bodies. More equant boudins have rotated less than elongate boudins (aspect ratios >3) and preserve the largest anticlockwise angles with the overall boudin train. Conversely, domino boudins are clockwise of overall boudin trains and have undergone clockwise rotation marked by left-stepping of adjacent boudins. Domino boudins display flanking folds which progressively open as the deformable boudin rotates towards the foliation and margins of the boudin lozenges locally become clockwise of flow. This 'unfolding' of deflected foliation, together with local reversals in the sense of shear around rotating boudins, is consistent with a clockwise vorticity associated with bulk dextral shear. These observations collectively indicate that bulk dextral shear with an additional component of pure shear operated across the shear zone and provides further insights into the kinematics of mid-crustal deformation.

Keywords: shear zone; intrusion; boudinage; folding; flanking folds; Caledonides

1. Introduction

Multiple sets of granitic pegmatite veins are recorded widely in the exhumed parts of many orogenic belts (e.g. Karlstrom et al., 1993; Carreras and Druguet, 1994; Henderson and Ihlen,

2004) and many are directly associated with crustal-scale shear zones which are often inferred to act as channel-ways that controlled magma emplacement (Holdsworth and Strachan 1988; Hutton 1988; D'Lemos et al., 1992; Ingram and Hutton, 1994, Brown and Solar, 1998a, b; 1999). These tabular granitic sheets are typically heterogeneously deformed by ductile deformation related to the host shear zone and the resulting structural styles give an indication of the viscosity or competence of the intrusive units relative to their host rocks (e.g. Ramsay and Huber 1983; 1987; Talbot, 1999). Diagnostic features associated with such deformed igneous sheets include buckle folds, cuspate-lobate structures, boudins and pinch-and-swell structures (e.g. Passchier et al., 2005; Druguet et al., 2008). The rotation of objects such as sheets and boudins in a host rock matrix and associated development of flanking folds of the foliation in the adjacent host rocks, additionally carries information about the sense of shear and vorticity of the shear zone deformation field (e.g. Passchier, 1990; 1991; 2001; Wiesmayr and Grasemann, 2005; Fossen et al., 2013). A number of studies have examined the relationships between more competent markers such as intrusions or veins and shear zone kinematics, from the viewpoint of theoretical stress and strain (e.g. Talbot, 1970; Passchier, 1990; Lacassin et al., 1993; Sassier et al., 2009), analogue modelling (e.g. Sengupta, 1983; Zulauf and Zulauf, 2005) and fieldwork (e.g. Druguet et al., 1997, 2008, 2009; Druguet, 2019; Skjernaa and Pedersen, 2000; Henderson and Ihlen, 2004; Passchier et al., 2005). Various textbooks also draw on the analogy of shearing of variably oriented intrusions to explain strain and deformation within different types of shear zones (e.g. Ghosh, 1993, p.161; Passchier and Trouw, 2005, p.151; Davis et al., 2011, p.597; Fossen, 2016, p.336).

In this paper, we describe well exposed examples of variably deformed granite-pegmatite sheets within the Torrisdale Vein Complex (TVC) that is spatially associated with shear zones in Neoproterozoic Moine metasedimentary rocks of N Sutherland, Scottish Caledonides (Figs. 1, 2) (Burns, 1994; Holdsworth et al., 2001; Strachan et al., 2010a, 2020). Specifically, we describe the geometric relationships between folded and boudinaged pegmatite sheets that were intruded into a localised strike-slip dominated shear zone that reworks older ductile thrusts. Examples of flanking folds, which are defined as 'deflections of planar or linear fabric elements in a rock alongside a cross-cutting object' (Passchier, 2001, p.951) are well developed adjacent to rotating pegmatite boudins and a range of structural relationships are recorded by pegmatite veins and apophyses injected at variable angles to the foliation. We propose a model involving dextral simple shear combined with foliation-normal pure shear shortening that creates extension parallel to strike. We broadly define this as a dextral general shear in a foliation-parallel subvertical shear zone (e.g. Dewey et al., 1998; Dewey et al., 1998; Fossen, 2016, p.411; Fossen et al., 2013, p.91). We discuss the overall kinematic patterns generated during the bulk dextral deformation of intrusions and consider the broader implications for understanding the regional development of vein complexes in orogenic belts.

2. Regional Setting

The rocks of the Moine Supergroup are arranged in a stack of east-dipping Scandian (Silurian) thrust sheets (Fig 1a; Barr et al., 1986; Strachan et al., 2002, 2010a; 2020). In north Sutherland, the main regional structures comprise, from west to east and structurally lowest to highest, the Moine, Naver, Swordly and Skinsdale thrusts (Fig. 1a, b) (Moorhouse and Moorhouse, 1988; Strachan and Holdsworth, 1988; Kocks et al., 2006; Holdsworth et al., 2006, 2007). Syndeformational metamorphic grade increases up-section from 450˚C and 5.0 kbar immediately above the Moine Thrust to 733˚C and 9.5 kbar in the immediate hangingwall of the Naver Thrust (Ashley et al., 2015; Mako et al., 2019).

Lithologically the Moine rocks of Sutherland comprise mainly psammites with subordinate pelites that locally preserve sedimentary features such as cross-bedding, slump folds and gritty to conglomeratic layers (Holdsworth, 1989; Holdsworth et al., 2001; Kocks et al., 2006; Alsop et al., 2010). In contrast, the overlying Naver nappe is dominated by migmatitic psammitic gneisses where all sedimentary features have been obliterated by high strain and intense metamorphic recrystallisation (Moorhouse and Moorhouse, 1988; Kinny et al., 1999). The Moine rocks are also interfolded and inter-thrust with Archaean orthogneisses which represent their depositional basement marked by locally preserved unconformities (Fig 1a, b) Peach et al., 1907; Holdsworth, 1989; Holdsworth et al., 2001; Friend et al., 2008).

The dominant structures in the Moine Nappe are locally referred to as 'D2' and are related to regional Scandian top-to the NW ductile thrusting (Fig 1a, b; Strachan and Holdsworth, 1988; Holdsworth, 1989; Holdsworth et al., 2001; Alsop et al., 2010). Reclined, tight to isoclinal D2 folds with southeasterly-dipping axial planes and curvilinear hinges are ubiquitous between the Moine and Naver thrusts and developed on all scales (e.g. Alsop and Holdsworth, 2007; 2012). D2 ductile thrusting and folding resulted in the development of a regional composite, gentle- to moderately- inclined, S0-S1-S2 (=Sn) foliation defined by aligned biotite and muscovite. This east to southeast-dipping fabric intensifies into blastomylonite associated with the D2 Naver ductile thrust. S2 carries a mineral extension and rodding lineation (L2) which trends between ESE and SSE and is sub-parallel to the axes of local F2 folds in most areas (Strachan et al., 2020).

Within the Moine Nappe, the D2 structures described above are deformed by local F3 buckle folds developed on all scales (Alsop and Holdsworth, 1993, 2007; Alsop et al., 1996). F3 fold axes and associated axial surfaces are variably oriented with respect to L2 and have been related to the development of flow perturbations during differential displacements along underlying D2 ductile thrusts (Holdsworth, 1990; Alsop and Holdsworth, 1993; 2002).

Displacements on the Naver and Skinsdale thrusts are associated with the emplacement of significant quantities of syn- to late-tectonic felsic melt (e.g. Holdsworth and Strachan, 1988; Kocks et al., 2006). The granites and pegmatites of the TVC are associated with the Naver Thrust and are most common in its immediate hangingwall around Torrisdale Bay and on Neave Island, where they locally form up to 50% of the outcrop (Figs. 1a, b, 2a). The veins appear to correlate with the Klibreck-Vagastie suite along strike to the south, members of which have yielded U-Pb zircon (CA-ID-TIMS) ages of 432-426 Ma (Strachan et al., 2020).

3. The Torrisdale Steep Belt

In the region around Torrisdale Bay where the TVC outcrops, ductile structures in the Moine and Naver nappes are reworked in a localised zone of later dextral general shear known as the Torrisdale Steep Belt (TSB, Figs. 1a, b, 2a; Holdsworth et al., 2001; Strachan et al., 2020). Here, the regional north-south-trending composite regional foliation, the Naver and Swordly thrusts, and F2 and F3 fold axial planes all steepen and become rotated anticlockwise into a NNW-trend (Fig. 2a-d). L2 is progressively overprinted by a strong mineral and rodding lineation (local L4) which plunges gently to the south-southeast, co-linear with local F2, F3 and F4 fold axes (Figs. 2a-e, 3a). Variably orientated fold hinges all progressively rotate towards the L4 lineation (Fig. 3b). A steep foliation is generally pervasive, although local zones of low strain preserve relic F2-F3 folds and lineations. The area of steep foliation and gently-plunging mineral lineations is dominated by dextral shearing that produces pegmatite sigmoids (Fig. 3c) (see Passchier and Trouw, 2005, p. 155 for definitions), together with σ (sigma) and δ (delta) porphyroclasts within the host gneisses and pegmatites (Fig. 3d, e) (Holdsworth et al., 2001; Strachan et al., 2020).

Metamorphic temperatures during dextral general shear were at least c. 500°C because L4 is defined by aligned hornblende and recrystallized aggregates of garnet (Burns, 1994; Holdsworth et al., 2001). It therefore seems unlikely that there was any substantial temporal break between the development of the TSB and the main phase of regional ductile thrusting (Strachan et al., 2020). On a regional scale, the anticlockwise swing and steepening of foliation in the TSB has been interpreted to reflect a wrapping of fabrics around the northern termination of a major basement inlier exposed immediately to the west of the TSB (the Borgie Inlier, Fig. 1a, b) (Strachan et al., 2020). This area of anomalous deformation has been exploited by large-scale ductile domino-like rotation and flattening (dextral 'bookshelf sliding') along the pre-existing shear zone foliation planes, as a result of the development of an inferred E-W trending lateral ramp to the Naver Thrust that is located offshore and further to the north (Fig. 1a, b) (Strachan et al., 2020).

The granitic pegmatites of the TVC are hosted in the lowest part of the Naver Nappe in amphibolites interbanded on a scale of 3-5 m with finely banded grey orthogneisses that are characterised by variable proportions of biotite, hornblende, garnet, quartz and feldspar (Burns 1994). These host rocks - the Druim Chuibhe Orthogneiss Complex – form a unit up to 350 m thick (Fig. 2a; Burns 1994). Preliminary geochemical data indicates that the complex is unlikely to be part of the local Archaean basement, and the various meta-igneous lithologies are viewed as most likely constituting a series of possibly contemporaneous pre-tectonic intrusions (Burns 1994).

The detailed petrography of the pegmatites within the TVC have been described by Holdsworth et al. (2001, p.47) who note that they comprise varying proportions of coarse grained (cm-mm scale) perthitic K feldspar, quartz and plagioclase (albite-oligoclase) together with minor components of garnet, muscovite, biotite, apatite, zircon and opaques. The central portions of intrusions are typically less strained and comprise equant feldspar crystals and interstitial quartz aggregates that are mostly undeformed with 120° intercrystalline boundaries. Holdsworth et al. (2001) note that extensive areas of myrmekite are developed adjacent to the K feldspar consistent with solid-state deformation. The margins of the intrusive veins are highly strained with penetrative L-S fabrics marked by aligned muscovite and locally biotite, together with recrystallized ribbons of quartz. This fabric wraps feldspar phenocrysts which are cracked and display undulose extinction indicating a component of brittle deformation. The fabric within the pegmatites forms strongly convergent fans around fold hinges (Fig. 3f, g), with pinched and cuspate margins around the inner arc of hinges (e.g. Fig. 3g), indicating that the pegmatites were more competent than the host gneisses during solid state deformation. Contemporaneous recrystallisation of quartz and brittle deformation of feldspar is generally taken to indicate solid state deformation under greenschist facies conditions (e.g. Passchier and Trouw, 2005).

4. Orientation and geometry of pegmatite intrusions

The TVC intrusions are sub-vertical to steeply NE-dipping, varying from veins a few cm thick to large sheet-like, anastomosing bodies up to 100 m thick, and are traceable laterally for up to 600 m [e.g. NC 694 608] (Figs. 2a, f). An L-S fabric defined by aligned quartz-feldspar aggregates is present within many intrusions and is parallel to the composite regional fabric in the host Moine rocks. The thickest intrusions are only deformed along their margins. Unambiguous temporal relationships between these intrusions and D2 and D3 folds are often difficult to establish because of the degree of overprinting during development of the D4 TSB. However, in areas of low D4 strain, intrusions cross-cut both the S0/S1 lithological banding, and D2 and D3 folds (Fig. 4a-f). Pegmatite intrusions cut both limbs of regional folds, with local deflections of foliation adjacent (<20 cm) to contacts interpreted as flanking folds generated by emplacement of pegmatites (Fig. 4a-f) (e.g. Butler and Torvela, 2018). Locally older (labelled 1) and younger (2) pegmatite veins cross-cut one another as well as regional folds and refolds within lower strain areas (Fig. 4f). Increasing D4 strain is marked by intense foliations, with markedly curvilinear fold hinges that display arcs of 160° around the sub-horizontal mineral lineations to create sheath folds (Fig. 4g). Although the majority of studied pegmatites were emplaced after regional D2 and D3 folding, but before D4, some of the larger sheets traceable for hundreds of meters (Fig. 2a) carry no fabrics and cut apparent D4 structures (Strachan et al., 2020). These late-stage undeformed sheets are believed to be intruded shortly after D4 and are not considered further in this study.

Previous accounts of the TVC are limited, but have suggested that the pegmatites are folded where they lie at high angles to the regional fabric, whilst those at a low angle are boudinaged, with structural asymmetries giving consistently dextral senses of shear viewed in sections parallel to L4 (Holdsworth et al., 2001). Others have suggested that pegmatites intruded clockwise of foliation are generally folded, while those that are anticlockwise are boudinaged (Strachan et al., 2010b, p. 252). A recent account of some of the pegmatite geometries, together with an interpretation of the timing of crystallisation and deformation has been provided by Butler and Torvela (2018). In order to test the various geometric assertions we have photographed and measured the trends of more than 260 steep to sub-vertical pegmatite intrusions within the TSB. Trend is defined as 'the azimuth of a geological feature' (Allaby, 2013, p.600) and is frequently used to delineate the orientation of igneous intrusions and dykes in a number of both older and more recent text books (e.g. Price and Cosgrove, 1990, p.74, 77; Pollard and Martel, 2020, p.382). We record trend where a planar pegmatite contact or foliation intersects a sub-horizontal outcrop surface thereby creating a linear intersection when measured from above (map-view). The steeply-dipping nature of pegmatites, coupled with the subdued topography and smoothed flat outcrop surfaces means that in this case trend and strike are broadly equivalent to one another. Our data were collected from a ~200 m square area centred on the sand-blasted western slopes of Druim Chuibhe at UK Grid: NC 68856160 [GPS: N58°31'23.600'' W4°15'10.730''] (please see supplementary file for GPS coordinates of all photograph localities) (Fig. 2a, f). The pegmatite intrusions here display an overall mean trend of 149º (N=261), while the foliation (Sn) adjacent to these intrusions has a mean trend of 150º. This statistical sub-parallelism between mean pegmatite and foliation trends masks a more complex relationship when the orientation of folded and boudinaged pegmatite intrusions are considered separately.

4.1. Trend of pegmatite fold trains

As both the intruded pegmatites and regional foliation have steep to sub-vertical attitudes within the TSB (Fig. 2a, b), it is appropriate to consider the orientations of these structures in terms of their trends relative to one another. The trend of a pegmatite fold train is measured by recording the azimuth of the enveloping surface that joins crests (or troughs) of adjacent fold hinges along the same margin of the pegmatite vein (e.g. Figs. 3h, 4a, 5a, c-e).

Pegmatite intrusions that are folded display a range of orientations, on average trending 157°, while the adjacent foliation (Sn) strikes 147°, meaning that folded pegmatites are statistically ~10º clockwise of the steep foliation (Table 1; Fig. 5b). In terms of field observations, 75% of folded pegmatites are developed clockwise of the adjacent Sn and trend 162°, while the remaining 25% of folded pegmatites are anticlockwise and trend 142º (Table 1). However, the foliation adjacent to these atypical anticlockwise folded pegmatites trends 154º and is itself therefore more clockwise than the overall mean (147º) foliation, i.e. pegmatites in these cases may have been intruding into local areas of anomalous striking foliation.

Pegmatite intrusions are deformed into steeply-plunging folds on a variety of scales from cm to metres and typically display ’Z’ asymmetry when viewed down plunge (Fig. 5a, c, d, e). The fold hinges generally plunge down the dip of the associated steep axial planes (inset stereonets in Fig. 5c, d, e) unless affected by shearing where steep fold hinges (labelled A) are rotated towards gently-plunging attitudes (labelled B) subparallel to the strike-slip lineation (Fig. 5a). The foliation in the adjacent quartzo-feldspathic gneiss and amphibolites does not typically record the same folding as it is oriented orthogonally to the inferred shortening direction.

4.2. Trend of pegmatite boudin trains

The trend of a pegmatite boudin train is measured by recording the azimuth of the enveloping surface that joins the flanks of adjacent boudins along the same margin of the pegmatite vein (see Goscombe et al., 2004) (e.g. Figs. 3h, 6a, f, g). Pegmatite intrusions are boudinaged on a variety of scales from cm to metres, with boudins best seen in gently-inclined to sub-horizontal outcrop surfaces that act as section views in the strike-slip dominated TSB (Fig. 6a-c, e-i). Boudinaged intrusions trend on average 143°, while the adjacent foliation (Sn) trends 152°, meaning that they are statistically ~9° anticlockwise of the steep foliation (Table 1; Fig. 6d). In the field, 83% of boudinaged pegmatites are developed anticlockwise of the adjacent Sn and trend 141°, while the remaining 17% are clockwise trending on average 153º (Fig. 6i). However, in these cases the foliation trends 145º and is itself therefore more anticlockwise than the overall mean (152º) foliation trend, i.e. once again, these pegmatites may have been intruding into local areas of anomalously striking foliation (Table 1). In a small number of cases, the pegmatites trending clockwise of foliation also display an atypical sense of sinistral shear suggesting that localised reversal in shear sense may develop (Fig. 6i).

The trends of folded and boudinaged pegmatite veins display distinct, if overlapping, patterns that are generally clockwise and anticlockwise of foliation (Sn), respectively (Fig. 7a-f). If the trend of regional foliation (Sn) deviates, then the trend of folded and boudinaged pegmatite vein shows a corresponding variation seemingly in order to maintain the obliquity relationship (Fig. 7e, f). The deviation in foliation trends may be a result of early F2-F3 folding, or variations in strain and/or the general slight swing in strike as the high-strain zone is traced from south to north in the Torrisdale area (Fig. 2a). Fold hinges within pegmatites generally plunge down the dip of their associated axial planes, and then display a rotation towards more gently-plunging attitudes associated with hinge tightening and strike-slip shear (hinge clusters marked ‘A’ and ‘B’ respectively in stereonets in Fig. 7h, i).

We have also investigated the % shortening in folded pegmatites, and the % extension in boudinaged pegmatites using simple line length measurements on the flat outcrop surfaces (e.g. Price and Cosgrove, 1990, p.9) and compared these values with the angle of obliquity that the pegmatite train makes with the foliation (Sn) (Fig. 8a-f). In folded pegmatite trains, the % shortening increases as the angle of clockwise obliquity with Sn becomes greater (Fig. 8a). Some folded pegmatites display ~80% shortening and form trains at high angles (>60°) to Sn, whereas pegmatites marked by <30% shortening are developed within 30° clockwise of Sn (Fig. 8 a-d). Although folded pegmatites are generally clockwise of Sn, some intensely shortened (~70%) pegmatites are preserved at greater angles (100°-120°) in an anticlockwise sense, i.e. they lie on the opposite side of the foliation-normal orientation so that the acute angle is actually anticlockwise to Sn (Fig. 8a). In boudinaged pegmatite trains, the % extension increases as the angle of anticlockwise obliquity with Sn reduces (Fig. 8e). Pegmatite trains at ~25° to Sn typically display ~10% extension, and this increases to >100% extension when pegmatite trains are ~5° anticlockwise of Sn (Fig. 8 e, f). Data suggest that the relationship between % extension and foliation obliquity is non-linear, with % extension increasing exponentially at obliquities of <10° (Fig. 8e).

4.3. Geometry of individual pegmatite folds

Analysis of the folded pegmatites reveals that they form across a variety of scales, with wavelengths ranging from cm to m; the latter is generally dependent on the thickness of the pegmatite (Fig. 9a, b). Fold hinges are predominantly steeply plunging, although those folds that are tightened or display pronounced shearing are rotated towards the sub-horizontal lineation (fold clusters ‘A’ and ‘B’ in stereonets, Fig. 9a, b). In general, fold hinges that have not been rotated display broadly parallel (Class 1B) geometries, where the folded layer maintains its orthogonal thickness around the fold hinge and limbs (Fig. 9a, b). Matching of marker layers on each side of pegmatite intrusions suggests that they opened in directions parallel to foliation irrespective of their present orientation (Figs. 5a, 9a). The general role of buckling suggested by the broadly parallel fold shapes (Fig. 9e) is consistent with the pegmatites being more competent than their host quartzo-feldspathic gneisses and amphibolites at the time of deformation, i.e. the pegmatites were not in a magmatic state.

In order to provide a more detailed analysis of folded pegmatite shapes we have undertaken a dip-isogon analysis (Fig. 9c, d) (e.g. Ramsay, 1967, p.363). In this method, dip isogons join points of equal dip on adjacent folded surfaces, t_0 is layer thickness measured along the axial surface, while t_α is orthogonal layer thickness measured at various angles (α - alpha) to the axial surface. Graphs normalise thicknesses by using t'_α (where $t'_\alpha = t_\alpha / t_0$) and plot this value against dip angle (α) to create a series of plots that can compared to a series of idealised curved that are used to differentiate different fold classes (Ramsay 1967, p. 366). Class 1 folds are marked by convergent dip isogons, Class 2 folds by parallel dip isogons, and Class 3 folds by diverging dip isogons (e.g. Ramsay 1967, p.365; see Fossen, 2016, p.263). The analysed folded pegmatites display convergent dip isogons and plots within the Class 1C field, where slight attenuation of the limbs relative to the hinge is observed (Fig. 9c, d). Such patterns are typical of buckle folds that have undergone a component of homogeneous flattening (Ramsay, 1967). If a homogenous flattening strain is applied to a parallel fold, then this additional strain is shown by the Z/X ratio of the superimposed theoretical strain ellipse, which reduces towards zero where the flattened parallel fold would approach a Class 2 similar fold shape (Ramsay 1967, his fig. 7.79; Price and Cosgrove, 1990, p.295). In the current study, analysis of pegmatite folds suggests Z/X ratios of between 0.9 to 0.5 (Fig. 9d).

Layer thickness (h), amplitude (*A*) and wavelength (λ) of single layer folds (rather than multi layers) may be measured in an attempt to estimate the strain and viscosity contrast between layers during folding (e.g. Schmalholz and Podladchikov, 2001; see also Hudleston and Treagus 2010). The thickness of a pegmatite (h) is measured orthogonal to the folded layer, while amplitude (*A*) is defined as half the distance from the trough to the crest of upright folds (e.g. Fig. 9f). Wavelength (λ) is defined as the distance between two points that occupy a similar position on the fold train (i.e. between adjacent synform hinges) (e.g. Fig. 9f). Schmalholz and Podladchikov (2001, p. 206) state that wavelength may also be measured as double the horizontal distance between neighbouring fold hinges (i.e. double the distance between antiform and synform fold hinges forming a fold pair).

In general, the amplitude (*A*) and wavelength (λ) of pegmatite folds increase together as expected in buckle folding (Fig. 9g). The amplitude / wavelength (*A*/λ) can be compared with layer thickness / wavelength (h/λ) on a strain contour map (Schmalholz and Podladchikov, 2001). For any fold where *A,* h and λ can be measured on the profile plane, estimates of the layer / matrix viscosity ratio and the bulk strain (in terms of % shortening) can be made by reading the position of data directly off the map (e.g. Fig. 9h). This technique assumes all the layer shortening is taken up by buckling with no out of plane movement or homogeneous layer thickening. Our analysed fold trains show linear data across a range of shortening values varying from ~55% to >70%, suggesting that viscosity contrasts of between 50 and 250 did not vary significantly during the folding of individual pegmatites, although estimated viscosity contrasts do change between different fold trains.

4.4. Geometry of individual pegmatite boudins

Individual boudins display a range of geometries that vary between lensoid-shaped ductile boudins to more blocky boudins potentially created during brittle 'tearing' of the competent body (Goscombe et al., 2004; Samanta et al., 2017) (Fig. 10a-f). The central parts of large (50cm thick) pegmatites remain undeformed (no grainsize reduction seen) despite boudinage. Blocky boudins are strongly wrapped by the foliation (Sn) (e.g. Fig. 10a, b) which is attenuated and folded around the boudin to create 'quarter-structures' consistent with dextral shear (Fig. 10c) (e.g. Fossen, 2016 p.346). The more blocky boudins can also display 'barrel' shapes where longer faces bow outwards while the two end terminations display asymmetric inward curving faces (Fig. 10b, d) (e.g. Samanta et al., 2017). Individual boudins are locally cut by shears or fractures that displace the boudin to create secondary dominoes (Fig. 10d), while 'ragged' intrusive pegmatite margins are sometimes preserved on the low-strain quadrants of equant boudins and along contacts protected from shearing (Fig. 10e).

The host metasediment contains scar folds where it has flowed to infill the boudin necks (Fig. 10f). As ductility increases, deformable boudins are marked by recrystallised tails of pegmatite extending off the 'corners' which are wrapped around the neighbouring boudin (Fig. 10g). Asymmetric boudins may display elongate 'tails' developing off the top left and bottom right quadrants (e.g. Fig. 11a-d), which is the mirror image to that typically developed in dextral shear (e.g. Fig. 3c), but entirely consistent with moderate non-coaxial deformation of barrel boudin shapes (e.g. Ghosh, 1993, his fig. 17.30b, p.414).

4.5. Geometry of pegmatite boudin trains

Individual boudins are frequently aligned to create elongate boudin trains that may be traced sub-parallel to the foliation for tens of metres (e.g. Figs. 4a, 6a). Although originally formed from a single pegmatite intrusive body, individual boudins may become entirely separated from one another such that they are now completely enveloped by the surrounding amphibolites and gneisses (Figs. 10a-f, 11a-e). As noted previously, such boudin trains are typically developed anticlockwise of the foliation trend (Figs. 6d, 7a-g, 8e, f, 11a-f). Boudin trains may be analysed by lining up the flanks of each adjacent boudin and comparing the trend of this enveloping surface (Goscombe et al., 2004) with: a) the regional foliation; and b) the amount and sense of rotation of individual boudins (see Ghosh, 1993 his fig. 17.28b).

In our examples, boudin trains are generally anticlockwise of foliation, while the long axis (L) of each individual boudin are preserved either:

i) parallel to the boudin train with no sense of lateral offset or stepping of adjacent boudins (e.g. Fig. 6a, b, c). These are representative of drawn boudins (e.g. Goscombe et al., 2004).

ii) oriented even more anticlockwise of the boudin train and the foliation and displaying en-echelon right-stepping of adjacent boudins (e.g. Figs. 6e, f, g, 8g, 10g). These are representative of shearband boudins (e.g. Goscombe et al., 2004).

iii) oriented clockwise of the boudin train and the foliation and displaying en-echelon left-stepping of adjacent boudins (e.g. Fig. 6h, 10h). These are representative of domino boudins (e.g. Goscombe et al., 2004). Overall, these various boudin geometries are consistent with dextral-dominated non-coaxial deformation.

We have also analysed the shape of individual boudins and compared this with the obliquity between the boudin and the foliation. The shape of a boudin may be defined by its length (L) and width (W), and this L/W ratio can be directly compared with the angle that L makes with Sn (Fig. 11a-f). More equant boudins display obliquity angles of up to 50°, whereas more elongate boudins with aspect ratios >3 are generally 10°-15° anticlockwise of Sn (Fig. 11f). Our results therefore show that boudins with larger aspect ratios plot closer to the shear plane marked by the foliation (Sn).

5. Progressive deformation and flanking folds next to pegmatite intrusions

5.1. Flanking folds

Flanking folds are localised deflections in bedding or foliation formed alongside a cross-cutting body such as an intrusion or boudin (e.g. Passchier 2001; Grasemann et al., 2003, 2018; Coelho et al., 2005). Within the case study, flanking folds are locally generated within quartzo-feldspathic gneisses adjacent to pegmatite boudins (Fig. 12a-h). They typically form within 20 cm of the pegmatite contact and display a systematic sense of overturning on each flank of the boudin. In shearband boudinage, synthetic slip along interboudin surfaces causes antithetic rotation of individual boudins (Fig. 12a, b). This results in flanking folds forming on the upper left and lower right quadrants of boudins where pegmatites originally cut across the regional foliation in the host gneisses (Fig. 12b).These relationships are consistent with anti-clockwise rotation of the shearband boudin during bulk dextral shear (Fig. 12a, b). In domino boudinage, antithetic slip along interboudin surfaces causes clockwise rotation of individual boudins during bulk dextral shear (Fig. 12c, d, e). Flanking folds are best developed at the widest point of domino boudins and in upper right and lower left quadrants which would otherwise be expected to lie within 'strain shadows' of boudins during dextral shear (Fig. 12c-g). Flanking folds may form on both margins of a boudin (e.g. Fig. 12c-e), or alternatively on just one side (Fig. 12h). In either case, local irregularities or steps along the contact may encourage flanking folds to develop (Fig. 12c).

Flanking folds were analysed by measuring the maximum angle of deflection (β) which the external foliation (Sn) undergoes from its regional trend, to where it intersects the boudin wall, and comparing this with the angle that the boudin long axis (L) makes with Sn (see Coelho et al., 2005, p.600) (Fig. 12h, i). We have chosen β to be the maximum angle of deflection, as this angle is not constant and varies along the flank of the boudin towards the terminations where it may reduce to zero (i.e. no deflection associated with flanking folds). The largest deflections of Sn (~165°) are associated with tight flanking folds along the margins of domino boudins that markedly cross-cut foliation by 20° (Fig. 12g). As the obliquity between the boudin long axis and Sn diminishes to ~5°, then the angle of deflection also reduces to ~90° (Fig. 12g).

5.2. Boudinaged folds

Although we have broadly divided pegmatites into folded and boudinaged bodies, it is entirely possible that pegmatites that were initially folded may be subsequently boudinaged as they enter the extensional field during progressive non-coaxial deformation (e.g. for a summary, see Fossen, 2016, p.51). Conversely, it should be noted that it is not possible to generate boudinage and then folding of that boudinage train in a single progressive deformation (Passchier and Trouw, 2005). Within the case study, a number of examples of pegmatite fold limbs that have undergone pinch and swell (e.g. Fig. 9c) or complete separation during boudinage are observed (e.g. Figs. 13a-h, 14a). Such boudinaged fold limbs are typically anticlockwise of the foliation (even if the overall fold train is clockwise). Analysis of boudinaged fold limbs reveals that the % extension compared to the angle of obliquity is no different from pegmatites that have simply undergone extension (Figs. 8e, 13g, h). Minor fold hinges that form part of boudinaged limbs may undergo a tightening and rotation towards the gently plunging lineation compared with fold hinges in the hinge of the larger fold (e.g. compare down-dip fold hinges (labelled 'A') with rotated fold hinges on boudinaged limbs (labelled 'B') shown in stereonets in Fig. 14a). The restriction of boudinage to fold limbs trending anticlockwise of Sn, and its absence from fold hinges, suggests that these structures were created during progressive non-coaxial deformation rather than separate deformational events.

5.3. Cross-cutting pegmatite veins and apophyses

Within igneous complexes, minor veins of slightly different ages may cross-cut one another, while apophyses of melt sourced from larger intrusions may inject into the surrounding host rock to create complex marginal networks. The relationship of cross-cutting minor veins and apophyses to surrounding folds and foliations is of interest as it potentially permits analysis of the evolution of structures during progressive deformation.

Within the case study, older pegmatite veins (labelled 1) are cross-cut by younger veins (labelled 2) (Figs. 4f, 13a-c). Older veins may be confidently traced as they generally reappear on the opposite margin of the younger intrusion (Figs. 13a-c, e, f), while distinct changes in crystal sizes and vein composition mark the cross-cutting contacts between different pegmatites (e.g. Fig. 13b). Where older veins (1) trend clockwise of Sn, they are subsequently folded (Fig. 13a-c) whereas younger veins (2) trending anticlockwise of foliation are later boudinaged (Fig. 13a-c). However, continued rotation of the boudin long axis may cause it to impinge on the older vein (1), causing a deflection and indentation (Fig. 13b). The limbs of folded older veins (1) may also undergo boudinage where they rotate into the extensional field during continued deformation (Fig. 13a-c). Older veins (1) that are injected at high angles to Sn display intense shortening, suggesting that significant deformation occurred during D4 and has been recorded by the veins (Figs. 7b, 13e). Older veins (1) that are cross-cut are generally folded, although examples of older boudinaged veins (1) being more anticlockwise of younger boudinaged veins (2) and associated foliation are occasionally observed (Fig. 13f). The typical lack of such cross-cutting boudinaged veins reflects the difficulty of observing interference between different boudin trains rather than their actual absence.

Within the case study, apophyses that are locally sourced and feed from pegmatites that are subsequently boudinaged also form (Fig. 14b) Such apophyses cannot be traced from the opposite margins of the 'feeder' vein and lack distinct differences in crystal size associated with older veins (see above). Where apophyses are clockwise of foliation then they are generally folded (Fig. 14b). More intensely folded apophyses display hinges that have rotated from down-dip directions ('A' hinges) towards more gently-plunging orientations ('B' hinges) closer to the gently-plunging lineation (stereonet inset in Fig. 14b). In some cases, apophyses cut directly across regional folds indicating that the apophysis post-dates regional F2-F3 folds that are locally protected from shearing around the margins of rigid intrusions (Fig. 14c). Further away from the source pegmatite, these cross-cutting pegmatite apophyses are themselves folded with steep hinges and a 'Z' asymmetry reflecting continued bulk dextral kinematics during progressive (D4) deformation (Fig. 14c). Matching of markers on either side of apophyses suggests that the veins opened orthogonally (Fig. 14c inset). In other cases, apophyses that are parallel to Sn are folded by flanking folds adjacent to the intrusion (e.g. Fig. 12c, d, e). Alternatively, apophyses cut across Sn, and are themselves folded by regional folds along the margins of the 'parent' pegmatite body (Fig. 14d). This suggests that some regional folds continued to tighten during D4 and affected both the host gneiss and apophyses to differing degrees, with apophyses therefore post-dating early regional folds. Finally, sites where apophyses branch from parent pegmatite bodies and intrude parallel to the foliation planes may locally coincide with where fold hinges later nucleate in pegmatites (Fig. 14e).

Apophyses injected from pegmatites that are boudinaged may be caught up in the continued rotation of the boudin, with clockwise spinning boudins creating locally intense isoclinal folds that become ‘wrapped’ around the boudin (Fig. 14f, g). Older veins (1) cut by younger veins (2) that are later boudinaged also form isoclinal folds that are tightly coiled around the rotating boudin (Fig. 14h, i). Such ‘spinning’ boudins are generally equant, although the sense of vorticity always appears to be clockwise reflecting bulk dextral shear (Fig. 14h, i). Clockwise rotating pegmatite boudins within bulk dextral shear will locally generate sinistral shear around their margins where the boudin rotates relative to the host. This local sinistral shear is supported by other shear sense such as σ porphyroclasts and creates local flanking folds with ‘S’ asymmetry opposite to the bulk shear sense (Fig. 14h, i).

6. Discussion

6.1. Geometry of pegmatite folds

Our estimates of the viscosity contrast of between 50 and 250 for the pegmatite and host gneisses (Fig. 9h) is similar to values obtained elsewhere in metamorphic and igneous rocks (e.g. Schmalholz and Podladchikov, 2001; Druguet et al., 2009: Llorens et al., 2013). The variations in viscosity contrasts between individual fold trains may reflect differences in the host lithology, together with temperature in the pegmatites at the time of deformation. All of the analysed pegmatite sheets here are of similar thickness in an attempt to reduce this thermal role (e.g. Fig. 9e, f).

Although it is frequently assumed that simple shear deformation of an inclined layer will create asymmetric folds verging in the direction of shear (e.g. Fossen, 2016, p.342), modelling studies suggest that “simple shear fold trains do not display a clear asymmetry” and that axial planes form normal to the fold train and are then rotated along with the fold train resulting in variable orientations (Llorens et al., 2013, p.209). Although very high shear strains may ultimately lead to an apparent reversal in fold vergence (e.g. Fossen, 2016, p.347), folds are generally considered to verge in the direction of shear. Folded pegmatites in the case study generally show ‘Z’ asymmetry that reflects dextral shear, while the Class 1C fold style suggests that the folded layers have not experienced sufficient shearing that would cause folds to become Class 2 (similar). Estimates of shortening around pegmatite folds are in the range of 55%-70% (Fig. 9h), while pegmatite fold trains generally trend at <45º to the foliation. Calculations of % shortening are based on line length measurements around folds and are thus minimum estimates that are subject to error where shortening has led to early thickening (rather than folding) of pegmatites. However, to create such % shortening by simple shear alone results in fold trains trending at ~45º or more to the foliation, even when the folded layering was initially inclined at just 14º to 27º from the shear direction (Llorens et al., 2013). If the marker layer was initially inclined 14º clockwise of the simple shear plane, and we assume a viscosity contrast of 100, then 50% and 70% shortening of the marker layer is achieved when it is rotated to ~29º ($\gamma \approx 2$) and ~51º ($\gamma \approx 3$) from the shear plane respectively (Llorens et al. 2013, p.213). In the case study, analysis of folded pegmatites suggests viscosity contrasts in the range of 50-250 (Fig. 9h) with 50% shortening achieved at an obliquity of ~35º, while 70% shortening forms angles of 50º with Sn representing the shear plane (Fig. 8a).These estimates are therefore broadly in-line with the simple shear models of Llorens et al (2013). However, greater values (80% - 90%) of shortening at high angles (~80º) to the shear plane (Fig. 8a), suggests that a foliation-normal pure shear component also operated during general shear.

A component of foliation-normal pure shear during general shear is supported by the Class 1C geometry of the pegmatite folds (Fig. 9d). Class 1C folds may be regarded as being created by a component of flattening associated with buckle folding (Ramsay 1967) and are therefore consistent with general shear across the high strain zone. Estimates of flattening across parallel folds suggest superimposed Z/X strain ratios of between 0.9 to 0.5 and are compatible with general shear (Fig. 9d).

6.2. Geometry of individual pegmatite boudins

Symmetrical boudins which do not experience slip on the interboudin surfaces are termed drawn boudins where there is ductile stretch of the competent layer, and torn boudins where this layer is cut by high-angle apparently brittle fractures to create angular or rectilinear boudins (Goscombe et al. 2004, p.751). In both cases, boudins are symmetrical with no apparent rotation, and the long axis of individual boudins remains parallel to the overall boudin train (e.g. Figs. 6a-c, 8f) (see Goscombe et al, 2004). There is a transition, marked by increasing asymmetry, from symmetrical drawn boudins to shearband boudins that form rhombohedral or sigmoidal shaped lenses with aspect ratios (*A*) that compare the length and width of the boudin displaying relatively high values (*A*=3-4) (e.g. Goscombe and Passchier, 2003; Goscombe et al., 2004). Shearband boudins exhibit obliquity relative to the main regional foliation and display synthetic movement and offset across the interboudin surface with respect to the bulk shear sense (e.g. Fig. 6e-g) (Goscombe and Passchier, 2003; Goscombe et al., 2004; Dabrowski and Grasemann, 2014; Rodrigues and Pamplona, 2018). Shearband boudins may develop wings that rotate into shear bands that separate boudins, with individual boudinaged blocks potentially displaying an antithetic sense of rotation with respect to bulk shear sense (e.g. Figs. 6f, 8g, 10g, 11a-e) (e.g. see Dabrowski and Grasemann, 2014 for a summary). There is also a transition from symmetrical torn boudins cut by high-angle interboudin faces to asymmetric domino boudins that generally display rhombohedral to rectangular shapes with low length to width aspect ratios (*A*=1-2) (Goscombe et al., 2004) (e.g. Fig. 10h). Domino boudins are marked by synthetic rotation of individual boudin blocks with respect to the bulk shear sense (e.g. Figs. 6h, 10h). Interboudin surfaces that separate adjacent boudins display an antithetic sense of slip created as neighbouring domino boudins rotate past one another (Goscombe et al., 2004; Dabrowski and Grasemann, 2014).

In the case study, pegmatite boudins collectively display a range of styles from ‘blocky’ shapes typically associated with more brittle deformation (e.g. Fig. 10a-f), to more lensoid and sigmoidal shapes characteristic of ductile behaviour (e.g. Fig. 10g) (see Fossen 2016, p.316 for a recent review). Rhombic-shaped boudins are observed (e.g. Fig. 10a-d) together with some layer-normal extension fractures cutting across boudins (e.g. Fig. 10c, d) indicating more brittle deformation and no evidence of melt leaking from torn boudins i.e. pegmatites were not in the magmatic state during deformation.

Barrel-shaped boudins, where longer faces bow outwards while the two end faces are asymmetric and inward curving (e.g. Figs. 10b, d, 11b) are considered to indicate that boudins are more competent than the matrix (e.g. Samanta et al., 2017) and initially formed with square sections that were deformable during rotation (Ghosh 1993, p.414, his fig.17.30b). Passchier and Druguet (2002) and Treagus and Lan (2000) suggest that barrelling is most likely to develop when boudin necks develop at ~90º to the length of the boudin. Ghosh (1993, p.414) shows that with increasing simple shear deformation, individual 'barrel-shaped' boudins not only rotate towards the shear direction, but also that the position of elongate or 'pointed' corners to the boudins switches from lower strains where the sheared corners point into the direction of shear (i.e. top left and lower right in dextral shear) (e.g. Figs. 10b, 11c, d) to more typical σ–type shapes at higher strains (Ghosh 1993, p.414, his fig. 17.30b, d) (e.g. Fig. 3c). Barrel-shaped geometries with concave end-faces suggest that boudins had a moderately high competence contrast with the matrix and the interboudin material (e.g. Samanta et al., 2017), while Dabrowski and Grasemann (2019) model classic barrel-shaped with intermediate viscosity ratios of ~10 and relatively low strains. The boudin geometries are therefore not consistent with melt pips that are 'squeezed' along high strain zones (e.g. Bons et al., 2004). However, the preservation of lenticular boudins (e.g. Fig. 6b, g, i) indicate that the competence contrast between pegmatites and the high-grade host gneisses may be rather limited in some cases (Ghosh, 1993, p.387).

6.3. Geometry of pegmatite boudin trains

The trend of a boudin train is defined by a line or surface joining the flanks of adjacent boudins to create an enveloping surface as defined by Goscombe et al. (2004) (Fig. 8g). The relative obliquity of this boudin train with the long axis (L) of individual boudins and the surrounding foliation has been analysed across a range of settings (e.g. Ghosh and Ramberg, 1977, Ghosh 1993; Goscombe and Passchier, 2003).

Where individual boudins rotate at a different rate to the overall boudin train, then en-echelon right-stepping or left-stepping boudin trains are created by slip along the interboudin surface (Ghosh 1993, p.405; Passchier and Druguet, 2002; Goscombe et al., 2004). The sense of synthetic or antithetic slip along the interboudin surface is largely controlled by the original orientation of this surface with respect to the walls of the intrusion, with interboudin surfaces inclined in the opposite direction to bulk shear sense being termed forward-vergent while those that are inclined in the same direction are referred to as backward-vergent respectively (Passchier and Druguet, 2002; Goscombe et al., 2004). In simple, pure or general shear, interboudin surfaces that display synthetic slip with respect to a bulk dextral shear sense will generate shearband boudins associated with a right-stepping en-echelon arrangement of adjacent boudin segments (e.g. Figs. 6f, 10g) (Passchier and Druguet, 2002; Goscombe et al., 2004). Conversely, interboudin surfaces that display antithetic slip with respect to a bulk dextral shear sense will generate domino boudins associated with a left-stepping en-echelon arrangement (e.g. Figs. 6h, 10h) (Passchier and Druguet, 2002; Goscombe et al., 2004).

If boudins are deformable, but more competent than the host, then the difference in rotation between individual boudins and the overall boudin train broadly increases with increasing competence contrast between the boudins and host (Ghosh 1993, p.409). Increasing the L/W aspect ratio of isolated boudins may also result in an increased rotation (Marques et al., 2007), although the amount of rotation is in general markedly reduced if adjacent boudins are in close proximity or direct contact with one another (Dabrowski and Grasemann, 2019). The proximity of adjacent boudins may therefore be the controlling influence on the amount of boudin rotation (Dabrowski and Grasemann, 2019).

Our observations from the TSB indicate that boudin trains are generally anticlockwise (<45°) of the foliation (Sn), with shearband boudins displaying en-echelon right-stepping (e.g. Figs. 6d-g, 10g) and domino boudins a left-stepping arrangement (e.g. Figs. 6h, 10h). Irrespective of boudin type, the greatest % extension is generally recorded by boudin trains at lower angles to Sn (Fig. 6a-g). The long axes of individual shearband boudins are anticlockwise of the overall trend of the boudin train, with more equant boudins recording the largest angles suggesting they have rotated less, or have rotated antithetically with respect to the bulk shear sense (Figs. 6f, 10g). Conversely, the long axes of individual domino boudins are clockwise of the overall trend of the boudin train, indicating they have rotated in a synthetic (clockwise) sense (Figs. 6h, 10h).

From the theoretical relationships described above, it can be seen that these geometric patterns are consistent with bulk dextral shear of the TVC. The present pattern may reflect the fact that pegmatites were initially intruded at variable angles to the foliation, but have subsequently rotated towards the dextral shear (X) direction resulting in the observed right-stepping and left-stepping arrangement of shearband and domino boudin trains respectively. This geometric relationship will also have been reinforced by pure shear acting across the shear zone (to create general shear) which encouragers further rotation of boudin trains towards the shear (X) direction. A component of pure shear across the TSB is also suggested by the increased % shortening of folded pegmatites at higher angles to Sn (see section 6.1.).

6.4. Flanking folds around pegmatite boudins

Flanking folds developed around boudins are widely recognised in shear zones (e.g. Passchier, 2001; Coelho et al., 2005). In the present study, flanking folds are formed around antithetically rotating shearband boudins (e.g. Figs. 12a, b, 15a), and also develop adjacent to domino boudins where they create overall Z shapes (e.g. Figs. 12c-g, 15b, c) suggesting that they may be reasonable indicators of dextral shear sense during non-coaxial progressive deformation (Butler and Torvela, 2018). Flanking folds form in the upper left and lower right quadrants of shearband boudins where the pegmatite originally cut foliation in the host gneisses (Fig. 15a). Conversely, flanking folds around domino boudins display the opposite pattern and generally form in the upper right and lower left quadrants (Fig. 15b, c). They are particularly well-preserved around the widest part of domino boudins and continue to develop on the protected 'leeward' side of boudins relative to the dextral shear couple (Figs. 12c-i, 15b, c).

The mechanism of formation of flanking folds has been discussed by several authors, with Passchier (2001, p. 957) suggesting that igneous intrusions alter the country rock margins via metasomatism. This locally increases the competence of the 'baked' margins and results in the external foliation being dragged around with the rotating boudin during subsequent deformation in what Grasemann and Stüwe (2001) term 'attached rims'. However, this interpretation of contact metamorphism and metasomatism does not explain the observation in the present case study that only the central and protected 'leeward' margin of each domino boudin generally display such flanking folds. In addition, the pegmatites were intruded into country rocks undergoing regional metamorphism with mineral lineations defined by aligned hornblende and recrystallized aggregates of garnet indicating temperatures of >500°C (Burns, 1994; Holdsworth et al., 2001). The pegmatites are therefore considered unlikely to create significant baked margins at such high regional temperatures, although fluids could locally alter the host-rock rheology along the contact while leaving little visible evidence of their presence. Flanking folds only developed towards the centre of each boudin have been simply attributed to ‘complex flow around developing boudins’ (Passchier, 2001, p.959, his fig. 6a). In the case study, the greatest angle of deflection (β) of the foliation into flanking folds is generally preserved at the widest part of boudin lozenges and then diminishes along the ‘leeward’ flank (Fig. 12c-i). It is notable that this reduction in the cut-off angle typically develops where the flank of the boudin lozenge is locally in a clockwise sense to the bulk dextral shear, although the long axis (L) of the domino boudin itself remains anticlockwise of flow (Figs. 12c-i, 15b, c). Grasemann and Stüwe (2001) suggest that foliation in attached rims adjacent to cross-cutting veins may locally be co-rotated with the more competent vein, with shear along the contact creating a drag effect resulting in ‘n-Type’ flanking folds.

We suggest that flanking folds initiate early in the deformation history as pegmatite veins are at first extended and then undergo boudinage as they rotate. As domino boudins undergo clockwise rotation, the flanking folds developed on boudin margins that have become clockwise of flow undergo extension and unfolding, thereby leading to a reduction in β in boudins as their long axis becomes sub-parallel to shear (Sn) (Figs. 12i, 15b, c). The observation that flanking folds are sometimes only developed on one margin of the boudin may also suggest that they may be created by boudin rotation enhancing and tightening folds on one flank, while the opposing margin underwent shear (e.g. Fig. 12h). This is similar to the mechanism proposed by Passchier (2001, his fig 8v’) where deflections along a cross-cutting structure are passively amplified during rotation. The application of a pure shear component during dextral shear may result in angular deflections where β <90° is reduced by the general shear.

6.4.a) Distinguishing flanking folds from regional folds adjacent to boudins

Distinguishing flanking folds from regional folds that pre-date intrusions can sometimes be problematical, as the style of regional folds may vary and appear atypical where they are protected from ongoing regional deformation in strain shadows formed along the flanks of an intrusion (see Druguet 2019 for a general review). In the ideal unambiguous situation, the earlier regional folds are themselves refolded and deflected by later flanking folds formed along the margins of the intrusion (Figs. 4c-f, 14j). In addition, intrusions may cut across both limbs of tight-isoclinal regional folds, whereas only the short limb of a monoformal flanking fold is truncated by the intrusion (Figs. 12 a-i, 14j). While the vergence of regional folds is dependent on larger scale tectonics, the asymmetry and style of flanking folds is very much dependent on the sense of truncation of foliation and vorticity around the intrusion. In this study, we observe that flanking folds are spatially restricted to within 20 cm of the intrusion, may nucleate adjacent to irregularities along the intrusive margin, and are generally best developed on the ‘leeward’ margins of the domino boudins (Figs. 12c-i, 14j). In this setting, the fold style displays a progressive opening of interlimb angles as the flanking fold is traced from the widest point of the boudin towards the tails. In addition, flanking folds frequently appear to form where the margin of the boudin has rotated to become clockwise of the general foliation, although the overall long axis of the boudin remains anticlockwise to it (Figs. 12c-g, 15b, c). The general correlation between the obliquity of the boudin with foliation, and the angle of deflection of the foliation in the flanking fold is also diagnostic of structures created during rotation of domino boudins (Fig. 12i). Distinguishing regional folds from flanking folds is critical when determining intrusive timing relationships and determining whether apophyses of melt remained in the system and potentially cut across later flanking folds.

6.5. Pegmatite apophyses and the state of crystallisation during deformation

Based on cross-cutting relationships, pegmatites may locally be divided in to older (1) and younger (2) veins (Fig. 13a-c, e, f). However, where veins can be separated, then they both cut the regional F2-F3 folds (e.g. Fig. 4f, 7b) and both are themselves reworked and refolded by D4 structures indicating that they were intruded at broadly the same time. Apophyses branching and feeding from pegmatite veins may be viewed as either part of this pre-existing anastomosing network of pegmatites that pre-date (D4) dextral shear, or alternatively as representing later stage melts that intruded synchronous with this deformation. In the latter scenario, melts intruded into active shear zones in Cap de Creus have previously been interpreted to create ‘pseudo-boudins’ where strings of magmatic ‘beads’ migrate along shear zones and therefore do not represent a single layer that was originally continuous (Bons et al., 2004). Alternatively, other workers have used the TVC as an example to suggest that crystallisation along the margins of intrusions formed a ‘strong rind’ that to some extent protects the ‘soft-centre’ where melt remained during deformation (Butler and Torvela, 2018). Clearly, these differing interpretations are significant as the state of melt within intrusions will affect the bulk rheology during crustal shearing (see Butler and Torvela, 2018 for a general discussion).

We now highlight some of the main observations from the case study relevant to the interpretation of the state of crystallisation of the TVC pegmatites at the time of deformation.

i) Extensive areas of myrmekite are developed adjacent to K feldspar grains and indicate solid state deformation (Holdsworth et al., 2001, p.47).

ii) Pegmatite grain sizes commonly decrease towards boudinaged necks consistent with recrystallisation linked to solid state deformation during shearing (e.g. Figs. 3c, d, e, 4b, 6h).

iii) Matching of marker layers across pegmatites suggests that most veins were tensile and opened orthogonally to their margins (e.g. Figs. 5a, e, 9a, 14c). This is less likely if melts were intruded obliquely into an actively shearing regime where they would be anticipated to accommodate some of the deformation and thereby display relative displacement of markers.

iv) Fabrics in folded pegmatites display convergent fans that extend across the entire thickness of the deformed veins indicating they were consistently more competent than the host (e.g. Figs. 3f, g, 14e inset).

v) The correlation between pegmatite layer thickness and fold wavelength suggests that the entire pegmatite vein was crystallised and more competent than the host gneisses during deformation (e.g. Fig. 9h). It is unlikely that this classical buckle fold relationship would persist if only the margins of the pegmatite vein had crystallised to create a ‘strong rind’ while the internal melt-rich areas formed ‘soft-centres’ that remained relatively weak (Butler and Torvela, 2018).

vi) Pegmatite veins generally display parallel (Class 1B) or sub-parallel (Class 1C) fold style consistent with buckling of competent layers (Fig. 9c, d) (see also Butler and Torvela, 2018). Such a fold style is less likely where shearing of melt-rich cores to pegmatite veins would lead to pronounced thinning of long limbs and thickening of short limbs of asymmetric folds.

vii) Viscosity contrasts of between 50 and 250 did not vary significantly during the folding of individual pegmatites (e.g. Fig. 9h). This suggests that the proportion of any melt present did not vary during folding and the veins were solid.

viii) Discrete failures marked by recrystallised finer-grained mylonites cut across over-tightened and rotated folds in the pegmatites (e.g. Figs. 5a inset, 7i inset). Localisation of deformation to create failed fold limbs is consistent with solid-state deformation.

ix) Barrel-shaped boudins with concave end-faces indicates that boudins were more competent than their host (e.g. Samanta et al., 2017; Dabrowski and Grasemann, 2019) and suggests that boudins were solid-state at the time of deformation, although with a potentially low competency contrast. No evidence is observed of melt escaping from the terminations of boudins or leaking from where boudins are cut across by later tear faults (e.g. Fig. 10a-e).

x) Pegmatite apophyses cross-cut early (F2-F3) regional folds (e.g. Fig. 4b), but are generally deformed by later (D4) structures and flanking folds (e.g. Figs. 12c, e, f, 14c). Some pegmatite apophyses cut early (F2-F3) regional folds which continued to tighten during D4 resulting in more limited shortening of the pegmatite (e.g. Fig. 14d). Despite careful searching, we observe no clear evidence of apophyses cutting across flanking folds developed around larger boudins that would demonstrate some melts remained and intruded post-boudinage.

xi) In some cases, we observe a coincidence of branching apophyses and fold hinges in pegmatites (e.g. Fig. 14e). This is interpreted to suggest that such ‘branching points’ represent areas of heterogeneity or ‘nodes’ where fold hinges are more likely to later nucleate.

xii) All older veins (1) connect directly with younger boudinaged veins (2) and there are no recorded examples of older veins cutting the necks between boudins (Fig. 13a-c, e). Passchier et al. (2005, p.76) note that while older veins can cross the suture between magma ‘beads’ that create the pseudo-boudins of Bons et al. (2004), they cannot cross the necked region between solid state boudins and must intersect the boudins themselves. As this distinguishing relationship is consistently observed in the case study, it thereby supports solid-state rather than magmatic state boudins.

xiii) Smaller-scale older veins and apophyses do not appear to display any less shortening than larger veins developed at the same angle to foliation. This suggests that both scales of veins suffered the same amount of shortening, with all veins and apophyses therefore intruded at the same approximate time in the deformation history.

In summary, while we cannot entirely rule out a small percentage of melt remaining in isolated pockets within deforming pegmatites of the TVC, our observations and reasoned interpretations collectively suggest that the pegmatites were intruded syn-late tectonically with respect to the regional ductile thrusting and prior to dextral shearing. During this local D4 event, they experienced predominantly solid-state deformation.

6.6. Overall patterns of extension and contraction recorded by pegmatite sheets

Given that the pegmatites were intruded at a variety of orientations within the TSB, and that viscosity contrasts between pegmatites and host gneisses and amphibolites could also locally vary, it is possible to provide only a general estimate of the relative components of simple shear and pure shear. Such assessments of shortening or extension are also complicated by layer-parallel shortening/extension that does not result in folding and boudinage of pegmatites, and the potential for out of plane movement. However, the development of pegmatite boudin trains anticlockwise of foliation (Sn) and pegmatite fold trains clockwise of Sn is entirely consistent with a dextral non-coaxial deformation where the foliation lies parallel to the regional shear plane and the finite extension direction lies sub-parallel to its strike (e.g. Fossen 2016, p.48) (Fig. 13i). Taking the orientation of folded and boudinaged pegmatite veins into account, and given the caveats noted above regarding variations in viscosity and deformation not recorded by folds and boudins, our data shown as variable line lengths and orientations (see Druguet et al., 2008, p.397 for method) are broadly consistent with general shear comprising $\gamma \approx 3$ and a pure shear component of 0.5 (Fig. 13i). Within such a scenario, both folded and boudinaged pegmatites trains will rotate towards the dextral shear direction (Figs. 13i, h, 16) (e.g. Fossen 2016, p.50, his fig. 2.31). This rotation progressively results in increasing % contraction in shortened pegmatites where they are at high angles to the shear plane, and increased stretching in boudinaged pegmatites where they approach the shear plane (Fig. 13i). Some pegmatites that were emplaced in the shortening field were initially folded, but during subsequent rotation they entered the stretching field resulting in boudinage of the fold limbs (Figs. 13d, g, h, 14a). The addition of a pure shear component to the deformation to create sub-simple shear (or general shear) may result in some markers developed close to the flow direction undergoing an anticlockwise ‘back rotation’, or actually rotating across the X axis (Fig. 13i) (Fossen 2016, p. 51, his fig. 2.32). Given an additional foliation-normal pure shear component, it is therefore entirely consistent that some 17% of boudinaged pegmatites form clockwise of Sn. Furthermore, a small number of atypical left-stepping shearband boudins also trend clockwise of foliation and are associated with sinistral shear (e.g. Fig 6i). These are interpreted to reflect localised reversals in shear sense within the predominantly dextral general shear regime. Similarly, intensely shortened pegmatites at high angles to Sn may rotate past the flow-normal to lie in the anticlockwise field (e.g. Fig. 9b). Development of 25% folded pegmatites only marginally (<20°) anticlockwise of Sn (Fig. 5b) may reflect intense shear and foliation-normal pure shear, but could also represent localised reversals in shear during the bulk dextral deformation, development of atypical short limbs on larger pegmatite folds (e.g. Fig. 8c), together with local ‘wrapping’ of fold trains around larger pegmatite bodies (e.g. Fig. 14e). Such folded pegmatite trains marginally anticlockwise of Sn are also likely to have suffered a component of post-folding boudinage within the extensional field (e.g. Fig. 13d, g, h, i), with similar ‘pinch and swell’ structures also observed in fold trains marginally clockwise of Sn (Figs. 5d, 7b, 9c).

7. Conclusions

Studies that provide a better understanding of the regional development of vein complexes in the mid-crustal portion of orogenic belts have a number of important implications. Examination of the detailed geometric relationships between veins permits an understanding of the bulk kinematic relationships and relative components of simple or pure shear in complex crustal shear zones. This provides greater insights into how deformation is partitioned in the crust. Clearly, the addition of significant volumes of melt into deforming crust has consequences for the strength of that crust and how it subsequently deforms (see recent discussion in Butler and Torvela, 2018). In addition, the exact timing of igneous intrusions, and whether veins are entirely synchronous or display a degree of diachroneity (e.g. Henderson and Ihlen, 2004) also has ramifications for their use in determining strain rates within deforming orogens (e.g. Sassier et al., 2009). While many of the issues surrounding these general objectives necessitate detailed field observations, our case study has allowed us to draw the following more specific conclusions.

7.1. Our observations of folded pegmatites from the Torrisdale Steep Belt are summarised in Figure 16 and reveal that pegmatite trains are typically (75%) clockwise of the adjacent foliation with fold trains that are at high angles to foliation displaying the greatest % shortening. Analysis of fold styles indicates viscosity contrasts between the pegmatites and host gneisses of 50 to 250 at the time of folding. Individual fold geometries are flattened parallel folds (Class 1C) and suggest up to 0.5 homogenous flattening. The marked 'Z' fold asymmetry, combined with pegmatites developed at high angles to the foliation showing the most significant shortening supports a general dextral shear interpretation. Matching of layers on each side of a pegmatite suggests that they opened normal to the vein walls, and therefore at high angles to the presumed shortening direction.

7.2. Our observations of boudinaged pegmatites from the Torrisdale Steep Belt are summarised in Figure 16 and reveal a range of 'blocky' barrel-shapes to lensoid geometries indicating a variety of deformation styles ranging from brittle to ductile respectively. Our data show that boudin trains are generally (80%) anticlockwise (<45°) of the foliation (Sn), with shearband boudins displaying en-echelon right-stepping and domino boudins a left-stepping arrangement. Irrespective of boudin type, the greatest % extension is generally recorded by boudin trains at lower angles to Sn. The long axes of individual shearband boudins are anticlockwise of the overall trend of the boudin train, with more equant boudins recording the largest angles suggesting they have rotated less, or have rotated antithetically with respect to the bulk shear sense. The long axes of individual domino boudins are clockwise of the overall trend of the boudin train, indicating they have rotated in a synthetic (clockwise) sense with respect to the dextral shear.

7.3. Flanking folds are developed adjacent to the upper left and lower right quadrants of shearband boudins, and in the 'opposite' upper right and lower left protected 'leeward' quadrants of domino boudins. These spatial and geometric relationships indicate that they are not an earlier fold related to regional tectonics, but are formed during creation and rotation of boudins during non-coaxial deformation. In domino boudins, the preferential development of flanking folds in strain shadows (behind the widest part of the boudin), coupled with their systematic asymmetry is consistent with clockwise rotation of domino boudins during bulk dextral shear. The reduction in the angle of deflection (β) of Sn as boudin margins become clockwise of dextral flow suggests a potential component of extension and unfolding of flanking folds during continued rotation.

7.4. Apophyses are locally sourced from pegmatites that form boudin trains or alternatively, may coincide with the hinges of buckle folds. Pronounced changes in pegmatite thickness represent heterogeneities that may focus later deformation. These include the nodes where apophyses branch from veins leading to later folding being focussed, together with thinning of pegmatites associated with boudinage focussing later refolding associated with spiral folds. These apophyses are subsequently deformed during dextral shear with apophyses clockwise of foliation undergoing folding while anticlockwise apophyses are boudinaged. Apophyses at high angles to foliation may display intense shortening Apophyses cut regional folds but are deformed by flanking folds developed around larger pegmatite boudins reflecting the ongoing deformation. The absence of apophyses cutting flanking folds, together with solid state deformation fabrics indicates that pegmatite intrusions were largely crystallised at the time of deformation forming the (D4) Torrisdale Steep Belt.

7.5. Pegmatite intrusions trending clockwise of foliation are generally folded, while those that are anticlockwise are boudinaged indicating bulk dextral deformation. The development of folds in some pegmatites that are anticlockwise of foliation highlights the complexity of natural systems linked to larger structures and potential local reversals in shear sense during bulk dextral shear. An additional component of foliation-normal pure shear across the shear zone to create general (or sub-simple) shear results in flattening of buckle folds that form Class 1C folds. Differing amounts of deformation recorded by pegmatites reflect slightly different orientations, resulting in variable amounts of hinge rotation towards the sub-horizontal shear direction. Despite the potential variation in viscosity contrasts between pegmatites and host gneisses, the pegmatite sheets display a remarkably consistent geometric arrangement illustrating the overarching control of the bulk kinematic regime.

Acknowledgements

Original fieldwork by GIA, RAS, REH involving mapping, data and sample collection was undertaken as part of NERC-BGS Academic Collaboration Programme during 1990-1993. IMB acknowledges a PhD studentship funded by Oxford Brookes University (1990-93). Aspects of this work were presented at the Highland Workshop (Edinburgh) and TSG (Durham) in April 2010 and January 2011 respectively. We thank Bernhard Grasemann and Sudipta Senguta for detailed and constructive reviews, together with Cees Passchier for efficient editorial handling. Finally, we would like to thank the participants of various conference field trips that have visited these localities for their lively discussion, together with numerous undergraduate field courses who have enjoyed the geology and hospitality of the north coast.

Figures

Figure 1 a) Geological map of Sutherland highlighting the major ductile thrusts. The locations of the Naver and related Torrisdale thrusts are also shown, as is the projected offshore continuation of the Naver Thrust and position of the detailed case study area around Torrisdale Bay (Fig. 2). b) Schematic 3-D cross section highlighting major thrusts and folds, together with the ductile domino model associated with dextral bookshelf sliding in the study area. See Fig. 1a for approximate location.

Figure 2 a) Geological map of the Torrisdale Bay area highlighting the major ductile thrusts that, in this area, have been reworked by dextral strike-slip deformation in the Torrisdale Steep Belt (TSB). The location of the Naver and Torrisdale Thrusts are indicated, as are some of the larger granite and pegmatite sheets. Stereonets show: b) poles to foliation (Sn) and L4 lineation (Ln); c) F2 fold hinges and poles to associated axial planes; d) F3 fold hinges and poles to associated axial planes; e) F4 fold hinges and poles to associated axial planes in folded pegmatites. f) View towards the south of Druim Chuibhe and the detailed study area (location shown in a).

Figure 3 a) Gently-plunging F4 fold hinge parallel to the lineation (Ln) within pegmatite veins. b) Folds within pegmatite veins display variable orientations associated with rotation towards the L4 lineation. Intense deformation within the Torrisdale Steep Belt leads to folding and shearing of pegmatites resulting in c) pegmatite sigmoids, and d), e) δ porphyroclasts. f) Hinge of folded pegmatite vein displaying a pinched and cuspate inner arc, and g) foliation wrapping the outer arc. In each case shown in f) and g), the fabric within the pegmatite vein displays a strongly convergent fan around the hinge. h) Pegmatite intrusion illustrating how enveloping surfaces are used to measure the trends of fold trains and boudin trains relative to foliation (Sn). Scale is provided by a 10 cm long chequered rule and a 15 mm diameter coin.

Figure 4 a), b) Pegmatite veins cross-cutting both limbs of tight-isoclinal regional folds with gently-plunging hinges sub-parallel to the shallow mineral lineations within amphibolites and gneisses of Druim Chuibhe In a), the general trend of the pegmatite fold train is defined by a pink line joining adjacent fold hinges to create a fold envelope along the pegmatite. c), d) Pegmatites cross-cutting both limbs of regional folds that are locally deflected by flanking folds developed along the margins of the intrusion. e) Tight regional fold cross-cut by the irregular intrusive margin of a pegmatite. Local steepening of the foliation and folding adjacent to the margin represents a flanking fold. f) Regional folds and refolds cut by pegmatites, with locally older (1) and younger (2) pegmatites cutting one another. g) Curvilinear sheath fold developed around the sub-horizontal L4 mineral lineation. Inset stereonet shows the orientation of fold hinge segments (red dots) measured at various positions (a-d) around the fold that collectively displays > 160° of hinge line curvature. Scale is provided by 10 cm long chequered rule.

Figure 5 a) Pegmatite vein displaying steeply-plunging parallel fold geometries and overall ‘Z’ asymmetry when viewed from above. The general trend (marked in pink) of such folded pegmatites is clockwise of the adjacent foliation (Sn) (highlighted in yellow). Inset photo shows detail of the opening direction of the pegmatite that is parallel to Sn in the host gneisses. Note the extreme thickening of the short limb and thrusting of the hinge consistent with dextral shear. b) Rose diagram highlighting the trends of folded pegmatite veins (N=105) relative to adjacent foliation (Sn). 75% of folded pegmatite veins are clockwise of Sn. c) Folding of ~50 cm thick pegmatite intrusion developed at a high angle to foliation (Sn). d) Buckle folding of pegmatite intrusion at moderate angles to foliation (Sn). The folded pegmatite displays pinch and swell on the fold limbs. e) Intense buckle folding of pegmatite at high angles to foliation (Sn). Inset stereonets (here and elsewhere) show individual fold hinges (red circles), poles to axial planes (red squares) and the mean axial plane (red great circle). Groups of fold hinges (labelled A) that plunge down the dip of the axial plane are in some instances tightened and rotated towards more gently-plunging attitudes (labelled B) during continued deformation. Scale is provided by a 10 cm long chequered rule and a 15 mm diameter coin.

Figure 6 a, b, c) Drawn pegmatite boudins developed anticlockwise of the foliation (Sn). In a), the trend of the boudinaged pegmatite train is defined by lining up the flanks of each adjacent boudin, and comparing this trend (shown by the dashed pale blue line) with the regional foliation (yellow line) d) Rose diagram highlighting the trends of boudinaged pegmatite veins (N=156) relative to adjacent foliation (Sn). 83% of boudinaged pegmatite veins are anticlockwise of Sn. e, f, g) Shearband boudins developed anticlockwise of the foliation (Sn) and marked by right-stepping necks along the boudin train. Note the more ‘blocky’ character of boudins bound by shears in e) and the more ductile deformation of boudins in f) and g). h) Domino boudins developed anticlockwise of the foliation (Sn) and marked by left-stepping necks along the boudin train. Inset photo in h) shows finer grained recrystallised tail to boudin. i) Example of shearband boudins that are left-stepping and form clockwise of foliation during localised sinistral shear. Scale is provided by a 10 cm long chequered rule and 15 mm diameter coin.

Figure 7 Structural data showing the relationships between folded pegmatite veins (N=105 in red) and boudinaged veins (N=156 in blue). Systematic relationships exist between the trends of boudinaged or folded pegmatite veins relative to foliation (Sn). a) Histogram showing trends of folded and boudinaged pegmatites. b) Photograph of boudinaged pegmatite trains trending anticlockwise of foliation (Sn), while folded pegmatites are clockwise. Note the boudinage of the fold limbs, and intense folding of high-angle pegmatite apophyses stemming from boudins. c) Histogram showing the relative obliquity between pegmatite veins and foliation (Sn) trends. d) Graph comparing the trend of boudinaged and folded pegmatites with the trend of adjacent foliation (Sn). Graphs showing how the difference in pegmatite and foliation (Sn) trends varies with e) the trend of pegmatites, and f) the trend of the foliation (Sn). Note that clockwise (Cw) trends are viewed as positive in each case. g) Right-stepping shearband boudin train (in blue) trending anticlockwise of foliation and fold train (in pink) trending clockwise of Sn. h) Photograph of pegmatite fold train trending clockwise of Sn while an anticlockwise trending boudin train is deflected where it crosses from amphibolite into gneisses. i) Moderately folded pegmatites with boudinage on fold limbs. Folded limbs are locally thrust and imbricated (inset). Inset stereonets in h) and i) show clusters of fold hinges (labelled A and B). Scale is provided by a 10 cm long chequered rule and a 15 mm diameter coin.

Figure 8 a) Graph showing how the % shortening recorded along fold trains varies with the clockwise (Cw) obliquity of the train to foliation (Sn) (N=25). Data measured from adjacent photos is located (b, c, d). Some high angle fold trains have passed through the foliation (Sn) normal to lie anticlockwise (A-Cw) of Sn. b) Photograph of folded pegmatite displaying 78.6% shortening and a 62° clockwise (Cw) obliquity to Sn. Data from this fold is shown on the graph (a). c) Intensely (92.7%) shortened pegmatite at 90° to Sn. d) Intensely shortened (68.8%) pegmatite displaying ‘Z’ folds while regional foliation shows ‘S’ folds. Obliquity is measured by a fold envelope line (in pink) joining adjacent fold hinges to create a general trend. e) Graph showing how the % extension recorded along boudin trains varies with the anticlockwise (A-Cw) obliquity of the train to foliation (Sn) (N=30). Data measured from adjacent photo f) and other figures is located. Blue triangles are data measured from boudinaged fold limbs and display no distinct difference to other boudin trains. f) Photograph showing how pegmatite boudin trains display anticlockwise obliquity to Sn, with individual drawn boudins remaining parallel to one another. g) Shearband boudins with individual boudin long axes developed anti-clockwise of the overall boudin train. Scale is provided by a 30 cm long hammer, 10 cm long chequered rule and a 15 mm diameter coin.

Figure 9 a) Centimetre-scale folded pegmatite vein trending 62° clockwise of foliation (Sn) and showing 50% shortening. Note the opening of the vein orthogonal to margins highlighted in the inset photo. b) Metre-scale folded pegmatite which displays a 117° obliquity (measured clockwise from Sn) and 67% shortening. In both a) and b), fold hinges on stereonet insets display rotations from down-dip orientations (labelled A) to more gently plunging attitudes (labelled B). c) Class 1C folded pegmatite vein that has undergone dip isogon analysis shown in d). Note pinch and swell structures on the fold limbs associated with flattening of the folds on the dip-isogon plot. e) f) Examples of fold styles in pegmatite veins that have been analysed in terms of g) amplitude and wavelength, and h) strain contour map developed by Schmalholz and Podladchikov (2001). Details of amplitude (*A*), wavelength (λ) and thickness (h) parameters are shown in f). Scale is provided by a 10 cm long chequered rule and a 15 mm diameter coin.

Figure 10 Individual boudins showing geometries that vary from more ‘brittle’ blocks with barrel shapes to ductile boudins displaying tails that wrap one another. Individual boudin blocks displaying a) foliation (Sn) wrapping around a rotating boudin, b) barrel-shape with concave end faces, c) quarter folds and tearing faults cutting boudins, d) antithetic tearing faults cutting domino boudins, e) Irregular intrusive contacts along boudin margins. f) Large boudin blocks with scar folds developed in necks of shearband boudins. g) Ductile shearband boudins displaying antithetic rotation and synthetic shearing along interboudin surfaces. h) Domino boudins marked by clockwise rotation and antithetic shear along sharp interboudin surfaces.

Scale is provided by a 30 cm long hammer, 10 cm long chequered rule, a 7 cm diameter lens cap and a 15 mm diameter coin.

Figure 11 a) Boudinaged pegmatite trains may be described in terms of lining up the flanks of each adjacent boudin and comparing this trend (shown by the dashed pale blue line) with the regional foliation (yellow line). Individual shearband boudins are labelled a-g and display long axes that are anticlockwise of the foliation (Sn) (see inset photos). The overall boudin train displays 108% extension. b-c) Examples of individual shearband boudins displaying antithetic rotation and shown in photo a). d), e) Photographs of shearband boudin trains with some labelled boudins shown in close-up inset photos. f) Graph comparing the boudin length – width (L/W ratio) with the anticlockwise (A-Cw) obliquity of the long axis to Sn from boudins displayed in a), d) and e). The graph shows that the L/W ratio varies with the obliquity to Sn of individual boudins. Scale in photographs is provided by a 30 cm long hammer and a 15 mm diameter coin.

Figure 12

a, b) Flanking folds developed around shearband boudins where the pegmatite margin originally cross-cut the regional foliation (Sn). Adjacent boudins display right-stepping and antithetic rotation. c, d, e) Flanking folds around deformable domino boudins are best developed where the boudin margin trends clockwise of general dextral flow, while the overall long axis of boudin remains anticlockwise to Sn. f, g) Examples of flanking folds developed on the protected 'leeward' margin of domino boudins that now trend clockwise of foliation (Sn). h) Photograph highlighting angle of obliquity of boudin to foliation (Sn) and angle of deflection of foliation (β) into flanking folds along the margin of the boudin. These parameters are compared on plot i) and show that the angle of Sn deflection reduces as the obliquity of the pegmatite margin to Sn also decreases.

Figure 13 a, b) Older pegmatite veins (1) are cut by younger pegmatites (2). The older veins are clockwise of foliation (Sn) and are folded during later deformation, whereas younger veins (2) are anticlockwise (A-Cw) and boudinaged. In c), older veins (1) are deformed by rotating boudins (2). d) Folded pegmatite with boudinaged limbs. Fold hinges preserve steep down-dip plunges (see stereonet inset). e) Older veins (1) that trend at high anticlockwise angles to foliation are cut across by younger pegmatites (2). f) Older veins (1) that trend at low anticlockwise angles to foliation are cut across by younger pegmatites (2). g); h) Folded pegmatites with limbs that are subsequently boudinaged. i) Best fit horizontal sectional finite strain ellipse (≈*XZ*) obtained from measuring the % extension or contraction of variably orientated veins (see Druguet et al. 2008 for details of technique). The data is superimposed on the simplified model of general dextral shear modified from Fossen (2016, p.51) and based on $\gamma \approx 3$ and a pure shear component of 0.5 (see text).

Figure 14 a) Folded pegmatites with limbs that are later boudinaged. On the inset stereonet, fold hinges rotate from steeper down-dip plunges (A) to gently plunging attitudes (B) on the sheared limbs. b) Apophyses injecting at high angles from boudins. c) Some thin pegmatite offshoots cross-cut regional folds with 'S' asymmetry. The cross-cutting pegmatite veins are themselves folded with 'Z' asymmetry reflecting bulk dextral shear. d) Pegmatite apophyses cross-cuts a regional fold pair. The apophyses is also shortened suggesting continued tightening of the regional fold during dextral general shear. e) Pegmatite veins are deformed by sinistral shear around the margins of clockwise rotating boudins during overall dextral kinematics. Apophyses that branch from pegmatite veins locally cross-cut Sn next to folds (inset). f) Pegmatite veins and boudins are marked by clockwise rotation associated with dextral shear. g) Folded and boudinaged pegmatite veins undergoing clockwise rotation associated with dextral shear. In h) and i), older veins (1) are refolded by rotating boudins (2) that have created local sinistral shear around the margins. j) Summary cartoon highlighting the interplay of a clockwise rotating domino boudin with regional folds and flanking folds.

Figure 15 Summary cartoons of flanking folds developed around a) deformable shearband boudins, b) deformable domino boudins, c) an individual domino boudin rotating during progressive dextral general shear. In a), shearband boudins display right-stepping across interboudin surfaces (IBS) with flanking folds forming on the upper left and lower right quadrants, whereas in b) domino boudins display left-stepping with flanking folds generated on the upper right and lower left quadrants In b) and c) domino boudins undergo clockwise rotation with flanking folds best preserved on the margins of the deformable boudin that are locally clockwise of foliation

Figure 16 Schematic summary cartoon of boudinaged pegmatite (in blue) and folded pegmatite (red) veins deformed in the dextral general shear zone forming the Torrisdale Steep Belt. Observations are developed across a range of scales from cm to hundreds of m and establish a consistent geometric and kinematic framework within the high strain zone.

Table 1. Geometric relationships between folded and boudinaged pegmatite veins developed clockwise (Cw) and anticlockwise (A-Cw) of adjacent foliation (Sn) at Druim Chuibhe (Fig. 2a).

	Folded Pegmatite	**Boudinaged Pegmatite**
Mean foliation (Sn) trend	147º (N=105)	152º (N=156)
Mean pegmatite vein trend	157º (N=105)	143º (N=156)
Mean pegmatite vein obliquity to Sn	10º Cw (N=105)	-9º A-Cw (N=156)
Mean pegmatite trending clockwise (Cw) of Sn	162º (N=79)	153º (N=26)
Mean pegmatite trending anticlockwise (A-Cw) of Sn	142º (N=26)	141º (N=130)

References

Allaby, M. 2013. A dictionary of geology and earth sciences. Oxford University Press. ISBN: 978-0-19-965306-5. 660pp. Oxford, UK.

Alsop, G.I., Holdsworth, R.E. 1993. The distribution, geometry and kinematic significance of Caledonian buckle folds in the western Moine Nappe, northwestern Scotland. Geological Magazine, 130, 353-362, doi: 10.1017/S0016756800020033.

Alsop, G.I., Holdsworth, R.E. 2002. The geometry and kinematics of flow perturbation folds. Tectonophysics, 350, 99-125, doi: 10.1016/S0040-1951(02)00084-7.

Alsop, G.I., Holdsworth, R.E. 2007. Flow perturbation folding in shear zones. In: Ries, A., Butler, R.W.H. & Graham, R.H. (eds) Global Tectonic Processes: The Legacy of Mike Coward. Geological Society, London, Special Publications, 272, 77-103, doi: 10.1144/GSL.SP.2007.272.01.06.

Alsop, G.I., Holdsworth, R.E. 2012. The three dimensional shape and localisation of deformation within multilayer sheath folds. *Journal of Structural Geology.* 44, 110-128.

Alsop, G.I., Holdsworth, R.E., Strachan, R.A. 1996. Transport-parallel cross folds within a mid-crustal Caledonian thrust stack, northern Scotland. Journal of Structural Geology, 18, 783-790.

Alsop, G.I., Cheer, D., Strachan, R.A., Krabbendam, M., Kinny, P.D., Holdsworth, R.E., Leslie, A.G. 2010. Progressive fold and fabric evolution associated with regional strain gradients: a case study from across a Scandian ductile thrust nappe, Scottish Caledonides. In: Law, R.D., Butler, R.W.H., Holdsworth, R.E., Krabbendam, M. & Strachan, R.A. (eds) Continental Tectonics and Mountain Building: The Legacy of Peach and Horne. Geological Society, London, Special Publications, 335, 255-274, doi: 10.1144/SP335.12.

Ashley, K.T., Thigpen, J.R., Law, R.D. 2015. Prograde evolution of the Scottish Caledonides and tectonic implications. Lithos, 224-225, 160-178, doi: 10.1016/j.lithos.2015.03.011.

Barr, D., Holdsworth, R.E., Roberts, A.M. 1986. Caledonian ductile thrusting in a Precambrian metamorphic complex: the Moine of north-western Scotland. Geological Society of America Bulletin, 97, 754-764, doi: 10.1130/0016-7606(1986)97<754:CDTIAP>2.0.CO;2.

Bons, P.D., Druguet, E., Hamann, I., Carreras, J., Passchier, C.W. 2004. Apparent boudinage in dykes. Journal of Structural geology 26, 625-636.

Brown, M., Solar, G.S., 1998a. Shear-zone systems and melts: feedback relations and self-organization in orogenic belts. J. Struct. Geol. 20, 211-227.

Brown, M., Solar, G.S., 1998b. Granite ascent and emplacement during contractional deformation in convergent orogens. J. Struct. Geol. 20, 1365–1393.

Brown, M., Solar, G.S., 1999. The mechanism of ascent and emplacement of granite magma during transpression: a syntectonic granite paradigm. Tectonophysics 312, 1-33.

Burns, I.M. 1994. Tectonothermal evolution and petrogenesis of the Naver and Kirtomy nappes, north Sutherland. PhD thesis, Oxford Brookes University.

Butler, R.W.H., Torvela, T. 2018. The competition between rates of deformation and solidification in syn-kinematic granitic intrusions: Resolving the pegmatite paradox. Journal of Structural Geology, 117, 1-13, doi: 10.1016/j.jsg.2018.08.013.

Carreras, J., Druguet, E., 1994. Structural zonation as a result of inhomogeneous noncoaxial deformation and its control on syntectonic intrusions: an example from the Cap de Creus area (Eastern-Pyrenees). J. Struct. Geol. 16, 1525–1534.

Coelho, S., Passchier, C., Grasemann, B. 2005. Geometric description of flanking structures. Journal of Structural Geology 27, 597-606.

Dabrowski, M., Grasemann, B., 2014. Domino boudinage under layer-parallel simple shear: Journal of Structural Geology, 68, 58-65.

Dabrowski, M., Grasemann, B., 2019. Numerical modelling of boudinage under pure shear: Implications for estimating viscosity ratios and finite strain from natural examples: Journal of Structural Geology, 126, 109-128.

Davis, G.H., Reynolds, S.J., Kluth, C.F. 2011. Structural Geology of Rocks and Regions. Wiley, New York. ISBN – 978-0-471-15231-6

D'Lemos, R.S., Brown, M., Strachan, R.A., 1992. Granite magma generation, ascent and emplacement within a transpressional orogen. J. Geol. Soc., Lond. 149, 487–490.

Druguet, E. 2019. Deciphering the presence of axial-planar veins in tectonites. Geoscience Frontiers 10, 2101-2115.

Druguet, E., Passchier, C., Carreras, J. Victor, P. den Brok S. 1997. Analysis of a complex high-strain zone at Cap de Creus, Spain. Tectonophysics 280, 31-45.

Druguet, E., Czeck, D.M., Carreras, J. Castano, L.M. 2008. Emplacement and deformation features of syntectonic leucocratic veins from Rainy Lake zone (Western Superior Province, Canada). Precambrian Research 163, 384-400.

Druguet, E., Alsop, G.I., Carreras, J. 2009. Coeval brittle and ductile structures associated with extreme deformation partitioning in a multilayer sequence. *Journal of Structural Geology* **31,** 498-511.

Fossen, H., Teyssier, C., Whitney, D.L. 2013. Transtensional folding. Journal of Structural Geology 56, 89-102.

Fossen, H. 2016. Structural Geology. 2nd Edition. Cambridge University Press, Cambridge, UK, p.510.

Friend, C.R.L., Strachan, R.A., Kinny, P.D. 2008. U-Pb zircon dating of basement inliers within the Moine Supergroup, Scottish Caledonides: implications of Archaean protolith ages. Journal of the Geological Society, London, 165, 807-815, doi: 10.1144/0016-76492007-125.

Ghosh, S.K. 1993. Structural Geology. Fundamentals and modern developments. Pergammon.

Ghosh, S.K., Ramberg, H. 1976. Reorientation of inclusions by combination of pure and simple shear. Tectonophysics 34, 1-70.

Goscombe, B.D., Passchier, C.W., 2003. Asymmetric boudins as shear sense indicators—an assessment from field data. Journal of Structural Geology 25, 575-589.

Goscombe, B.D., Passchier, C.W., Hand, M., 2004. Boudinage classification: endmember boudin types and modified boudins structures. J. Struct. Geol. 26, 739–763.

Grasemann, B., Stüwe, K., 2001. The development of flanking folds during simple shear and their use as kinematic indicators. Journal of Structural Geology 23, 715-724.

Grasemann, B., Stüwe, K., Vannay, J-C. 2003. Sense and non-sense of shear in flanking structures. Journal of Structural Geology 25, 19-34.
Grasemann, B., Dabrowski, M., Schöpfer, M.P.J., 2018. Sense and non-sense of shear reloaded. Journal of Structural Geology 27, 249-264.

Henderson, I.H.C., Ihlen, P.M., 2004. Emplacement of polygeneration pegmatites in relation to Sveco-Norwegian contractional tectonics: examples from southern Norway. Precambrian Research 133, 207–222.

Holdsworth, R.E. 1989. The geology and structural evolution of a Caledonian fold and ductile thrust zone, Kyle of Tongue region, Sutherland, northern Scotland. Journal of the Geological Society, London, 146, 809-823, doi: 10.1144/gsjgs.146.5.0809.

Holdsworth, R.E. 1990. Progressive deformation structures associated with ductile thrusts in the Moine Nappe, Sutherland, N. Scotland. Journal of Structural Geology, 12, 443-452.

Holdsworth, R.E., Strachan, R.A. 1988. The structural age and possible origin of the Vagastie Bridge granite and associated intrusions, central Sutherland. Geological Magazine, 125, 613-620, doi: 10.1017/S0016756800023426.

Holdsworth, R.E., Strachan, R.A., Alsop, G.I. 2001. Geology of the Tongue District. Memoir of the British Geological Survey, HMSO, ISBN-10: 0118845489.

Holdsworth, R.E., Strachan, R.A., Alsop, G.I., Grant, C.J., Wilson, R. 2006. Thrust sequences and the significance of low-angle, out-of-sequence faults in the northernmost Moine Nappe and Moine Thrust Zone, NW Scotland. Journal of the Geological Society, London, 163, 801-894, doi: 10.1144/0016-76492005-076.

Holdsworth, R.E., Alsop, G.I., Strachan, R.A. 2007. Tectonic stratigraphy and structural continuity of the northernmost Moine Thrust Zone and Moine Nappe, Scottish Caledonides. In: Ries, A., Butler, R.W.H. & Graham, R.H. (eds) Global Tectonic Processes: The Legacy of Mike Coward. Geological Society, London, Special Publications, 272, 124-144, doi: 10.1144/GSL.SP.2007.272.01.08.

Huddleston, P.J., Treagus, S.H. 2010. Information from folds: A review. Journal of Structural Geology 32, 2042-2071.

Hutton, D.H.W., 1988. Granite emplacement mechanisms and tectonic controls: inferences from deformation studies. Trans. R. Soc. Edinb.: Earth Sci. 79, 245–255.

Ingram, G.M., Hutton, D.H.W. 1994. The Great Tonalite Sill: emplacement into a contractional shear zone and implications for Late Cretaceous to early Eocene tectonics in southweastern Alaska and British Columbia. Geological Society of America Bulletin, 106, 715-728.

Karlstrom, K.E., Miller, C.F., Kingsbury, J.A., Wooden, J.L. 1993. Pluton emplacement along an active ductile thrust zone, Piute Mountains, southeastern California: Interaction between deformational and solidification processes. GSA Bulletin 105, 213–230.

Kinny, P.D., Friend, C.R.L., Strachan, R.A., Watt, G.R., Burns, I.M. 1999. U—Pb geochronology of regional migmatites, East Sutherland, Scotland: evidence for crustal melting during the Caledonian orogeny. Journal of the Geological Society, London, 156, 1143-1152, doi: 10.1144/gsjgs.156.6.1143.

Kocks, H., Strachan, R.A., Evans, J.A. 2006. Heterogeneous reworking of Grampian metamorphic complexes during Scandian thrusting in the Scottish Caledonides: insights from the structural setting and

U-Pb geochronology of the Strath Halladale Granite. Journal of the Geological Society, London, 163, 525-538, doi: 10.1144/0016-764905-008.

Lacassin, R., P. H. Leloup, P. Tapponnier, P., 1993. Bounds on strain in large Tertiary shear zones of SE Asia from boudinage restoration, J. Struct. Geol., 15, 677– 692, doi:10.1016/0191-8141(93)90055-F.

Llorens, M-G., Bons, P.D., Griera, A., Gomez-Rivas, E., Evans, L.A. 2013. Single layer folding in simple shear. Journal of Structural Geology 50, 209-220.

Mako, C.A., Law, R.D., Caddick, M.J., Thigpen, J.R., Ashley, K.T., Cottle, J., Kylander-Clark, A. 2019. Thermal evolution of the Scandian hinterland, Naver nappe, northern Scotland. Journal of the Geological Society, London, 176, 669-688, doi: 10.1144/jgs.2018-224.

Marques, F.O., Schmid, D.W., Andersen, T.B. 2007. Applications of inclusion behaviour models to a major shear zone system: The Nordfjord-Sogn Detachment Zone in western Norway. Journal of Structural Geology 29, 1622-1631.

Moorhouse, S.J., Moorhouse, V.E. 1988. The Moine Assemblage in Sutherland. In: Winchester, J.A. (ed) Later Proterozoic Stratigraphy in the Northern Atlantic Regions. Blackie, Glasgow, p. 54-73, ISBN: 978-1-4615-7344-9.

Passchier, C.W., 1990. Reconstruction of deformation and flow parameters from deformed veins sets. Tectonophysics 180, 185–199.

Passchier, C.W., 1991. The classification of dilatant flow types. Journal of Structural Geology 13, 101-104.

Passchier, C.W., 2001. Flanking folds. Journal of Structural Geology 23, 951-962.

Passchier, C.W., Druguet, E. 2002. Numerical modelling of asymmetric boudinage. Journal of Structural Geology 24, 1789-1803.

Passchier, C.W., Trouw, R.A.J. 2005. Microtectonics. 2nd Edition. Springer.

Passchier, C.W., Zhang, J.S., Konopasek, J. 2005. Geometric aspects of synkinematic granite intrusion into a ductile shear zone – and example from the Yunmengshan core complex, northern China. In: Bruhn, D., Bulini, L. (Editors) High-strain zones: Structure and Physical Properties. Geological Society, London, Special Publications 245, 65-80.

Peach, B.N., Horne, J., Gunn, W., Clough, C.T., Hinxman, L.W. 1907. The geological structure of the NW Highlands of Scotland. Memoirs of the Geological Survey of Scotland, HMSO, Glasgow.

Price, N.J., Cosgrove, J.W. 1990. Analysis of Geological Structures. Cambridge University Press. 502pp.

Ramsay, J.G. 1967. Folding and Fracturing of Rocks. McGraw-Hill, New York. 568pp.

Ramsay, J.G., Huber M.I. 1983. The techniques of modern structural geology. Volume 1: Strain analysis. Academic Press London. 1-308p.

Ramsay, J.G., Huber M.I. 1987. The techniques of modern structural geology. Volume 2: Folds and Fractures. Academic Press London. 309-700p.

Rodrigues, B.C., Pamplona, J. 2018. Boudinage and shearband boudins: A meso to micro-scale tool in structural analysis. Journal of Structural Geology 114, 280-287.

Samanta, S.K., Majumder, D.B., Sarker, G., 2017. Geometry of torn boudin – An indicator of relative viscosity. Journal of Structural Geology 104, 21-30.

Sassier, C., P. H. Leloup, D. Rubatto, O. Galland, Y. Yue, Lin, D., 2009. Direct measurement of strain rates in ductile shear zones: A new method based on syntectonic dikes, J. Geophys. Res., 114, B01406, doi:10.1029/2008JB005597.

Schmalholz, S.M., Podladchikov, Y.Y. 2001. Strain and competence contrast estimation from fold shape. Tectonophysics 340, 195-213.

Sengupta, S. 1983. Folding of boudinaged layers. Journal of Structural Geology 5, 197-210.

Skjernaa, L., Pedersen, S. 2000. Late Sveconorwegian monzonitic dykes in the Setesdalen area of Central South Norway: Examples of structures in dykes and their indications of accumulated strain. *Bulletin of the Geological Society of Denmark*. Vol. 46, pp. 203–223.

Strachan, R.A., Holdsworth, R.E. 1988. Basement-cover relationships and structure within the Moine rocks of central and southeast Sutherland. Journal of the Geological Society, London, 145, 23-36, doi: 10.1144/gsjgs.145.1.0023.

Strachan, R.A., Smith, M., Harris, A.L., Fettes, D.J. 2002. The Northern Highland and Grampian terranes. In: Trewin, N. (ed) Geology of Scotland (4th edition): Geological Society, London, p. 81-147, ISBN: 1862391262 9781862391260.

Strachan, R.A., Holdsworth, R.E., Krabbendam, M., Alsop, G.I. 2010a. The Moine Supergroup of NW Scotland: insights into the analysis of polyorogenic supracrustal sequences. In: Law, R.D., Butler, R.W.H., Holdsworth, R.E., Krabbendam, M. & Strachan, R.A. (eds) Continental Tectonics and Mountain Building: The Legacy of Peach and Horne. Geological Society, London, Special Publications, 335, 233-254, doi: 10.1144/SP335.11.

Strachan, R.A., Holdsworth, R.E., Friend, C., Burns, I., Alsop, G.I. 2010b. Excursion 13, North Sutherland. In: Strachan, R.A., Alsop, G.I., Friend, C. & Miller, S. (Editors). An excursion guide to the Moine geology of the Northern Highlands of Scotland. Pages 231-265. Published by NMSE-Publishing Ltd. Edinburgh. ISBN: 9781905267330.

Strachan, R.A., Alsop, G.I., Ramezani, J., Frazer, R.E., Burns, I., Holdsworth, R.E. 2020. Patterns of Silurian deformation and magmatism during sinistral oblique convergence, northern Scottish Caledonides. Journal of the Geological Society, 177, 893-910.

Talbot, C. J. 1970. The minimum strain ellipsoid using deformed quartz veins. Tectonophysics 9, 47-76.

Talbot, C. J. 1999. Can field data constrain rock viscosities? Journal of Structural Geology 21, 959-967.

Treagus, S.H., Lan, L. 2000. Pure shear deformation of square objects, and applications to geological strain analysis. Journal of Structural Geology 22, 105-122.

Wiesmayr, G., Grasemann, B. 2005. Sense and non-sense of shear in flanking structures with layer-parallel shortening: implications for fault-related folds. Journal of Structural Geology 27, 249-264.

Zulauf, J., Zulauf, G. 2005. Coeval folding and boudinage in four dimensions. Journal of Structural Geology 27, 1061-1068.

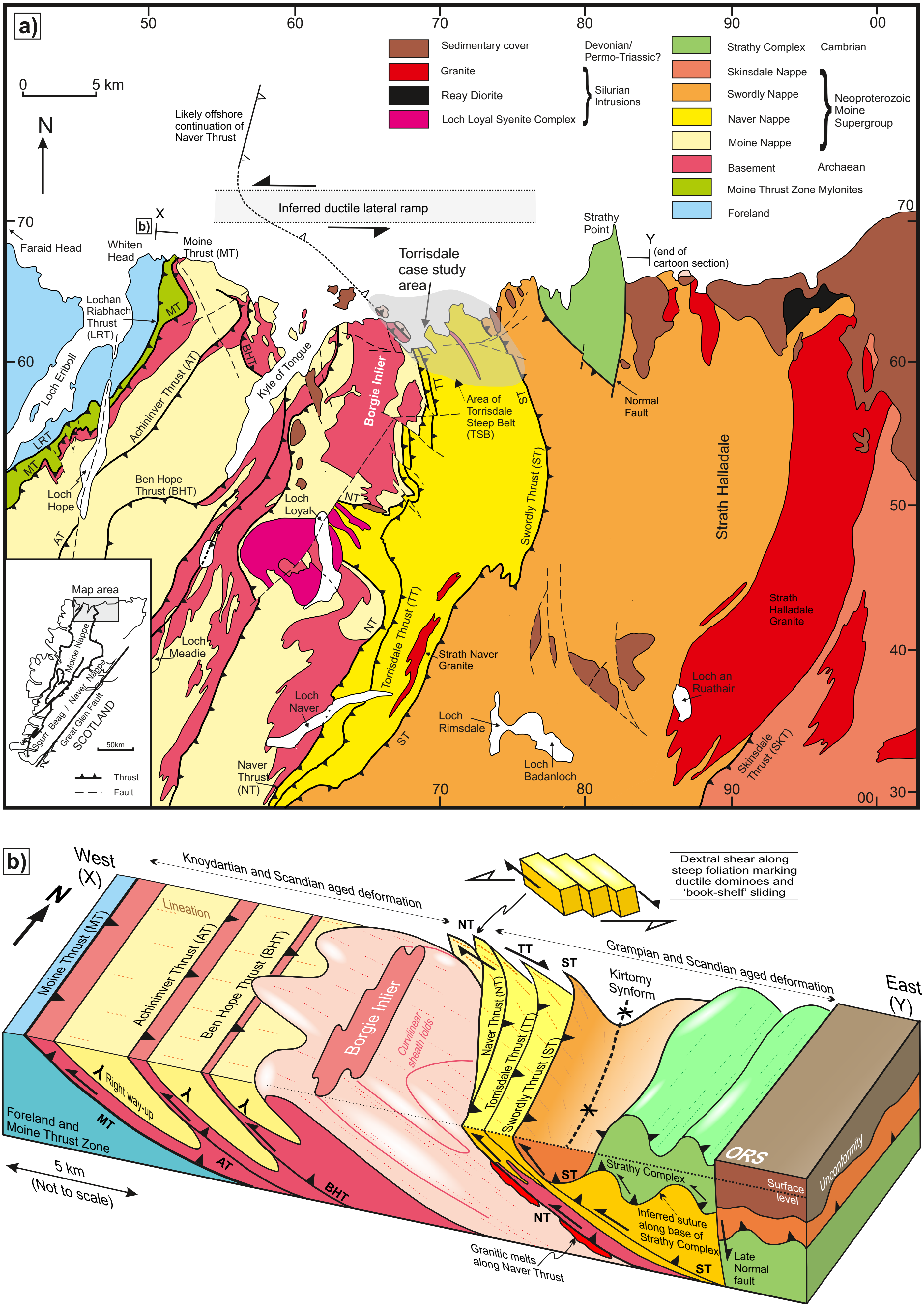
a)
50
60
70
80
90
00
0
5 km
N
Sedimentary cover
Devonian/ Permo-Triassic?
Granite
Reay Diorite
Loch Loyal Syenite Complex
Silurian Intrusions
Strathy Complex
Cambrian
Skinsdale Nappe
Swordly Nappe
Naver Nappe
Moine Nappe
Neoproterozoic Moine Supergroup
Basement
Archaean
Moine Thrust Zone Mylonites
Foreland
Likely offshore continuation of Naver Thrust
Inferred ductile lateral ramp
70
X
b)
Faraid Head
Whiten Head
Moine Thrust (MT)
Torrisdale case study area
Strathy Point
Y
(end of cartoon section)
Lochan Riabhach Thrust (LRT)
MT
60
Loch Eriboll
LRT
MT
Achininver Thrust (AT)
BHT
Kyle of Tongue
Borgie Inlier
TT
Area of Torrisdale Steep Belt (TSB)
ST
Normal Fault
60
Loch Hope
Ben Hope Thrust (BHT)
AT
Loch Loyal
NT
Swordly Thrust (ST)
Strath Halladale
50
Map area
Moine Nappe
Naver Nappe
Sgurr Beag / Naver
Great Glen Fault
SCOTLAND
50km
Thrust
Fault
Loch Meadie
NT
Torrisdale Thrust (TT)
Strath Naver Granite
Strath Halladale Granite
40
Loch Naver
ST
Loch Rimsdale
Loch an Ruathair
Naver Thrust (NT)
Loch Badanloch
70
80
90
Skinsdale Thrust (SKT)
00
30
b)
West (X)
N
Knoydartian and Scandian aged deformation
Dextral shear along steep foliation marking ductile dominoes and ‘book-shelf’ sliding
NT
TT
ST
Grampian and Scandian aged deformation
East (Y)
Lineation
Moine Thrust (MT)
Achininver Thrust (AT)
Ben Hope Thrust (BHT)
Borgie Inlier
Curvilinear sheath folds
Naver Thrust (NT)
Torrisdale Thrust (TT)
Swordly Thrust (ST)
Kirtomy Synform
Right way-up
MT
AT
BHT
Foreland and Moine Thrust Zone
ST
Strathy Complex
ORS
Surface level
Unconformity
NT
Inferred suture along base of Strathy Complex
ST
Late Normal fault
Granitic melts along Naver Thrust
5 km
(Not to scale)

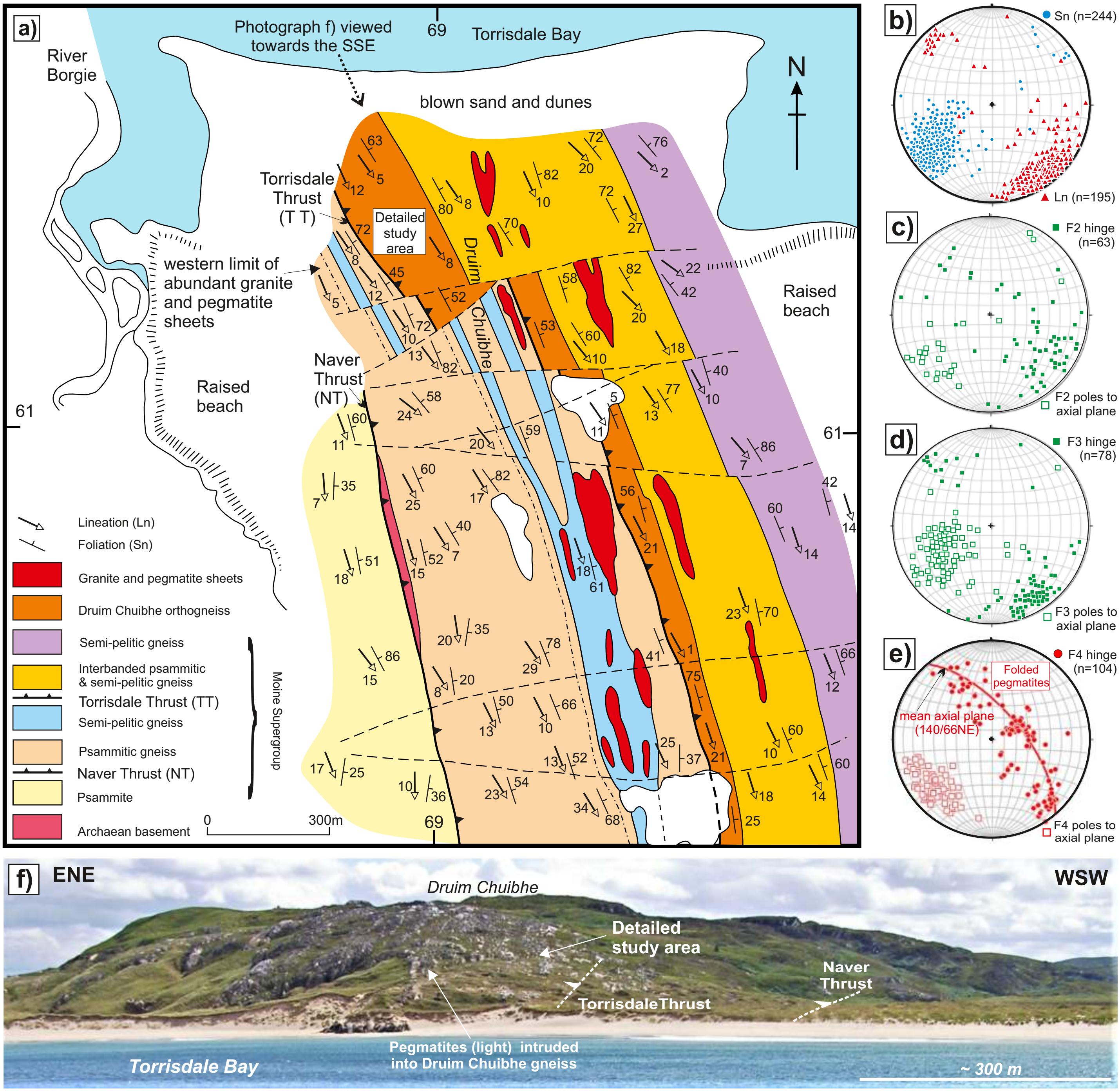a)
Photograph f) viewed towards the SSE
69
Torrisdale Bay
River Borgie
blown sand and dunes
N
Torrisdale Thrust (T T)
Detailed study area
Druim Chuibhe
western limit of abundant granite and pegmatite sheets
Raised beach
Naver Thrust (NT)
61
Raised beach
61
Lineation (Ln)
Foliation (Sn)
Granite and pegmatite sheets
Druim Chuibhe orthogneiss
Semi-pelitic gneiss
Interbanded psammitic & semi-pelitic gneiss
Torrisdale Thrust (TT)
Semi-pelitic gneiss
Psammitic gneiss
Naver Thrust (NT)
Psammite
Archaean basement
Moine Supergroup
0
300m
69
b)
Sn (n=244)
Ln (n=195)
c)
F2 hinge (n=63)
F2 poles to axial plane
d)
F3 hinge (n=78)
F3 poles to axial plane
e)
F4 hinge (n=104)
Folded pegmatites
mean axial plane (140/66NE)
F4 poles to axial plane
f)
ENE
WSW
Druim Chuibhe
Detailed study area
TorrisdaleThrust
Naver Thrust
Pegmatites (light) intruded into Druim Chuibhe gneiss
Torrisdale Bay
~ 300 m

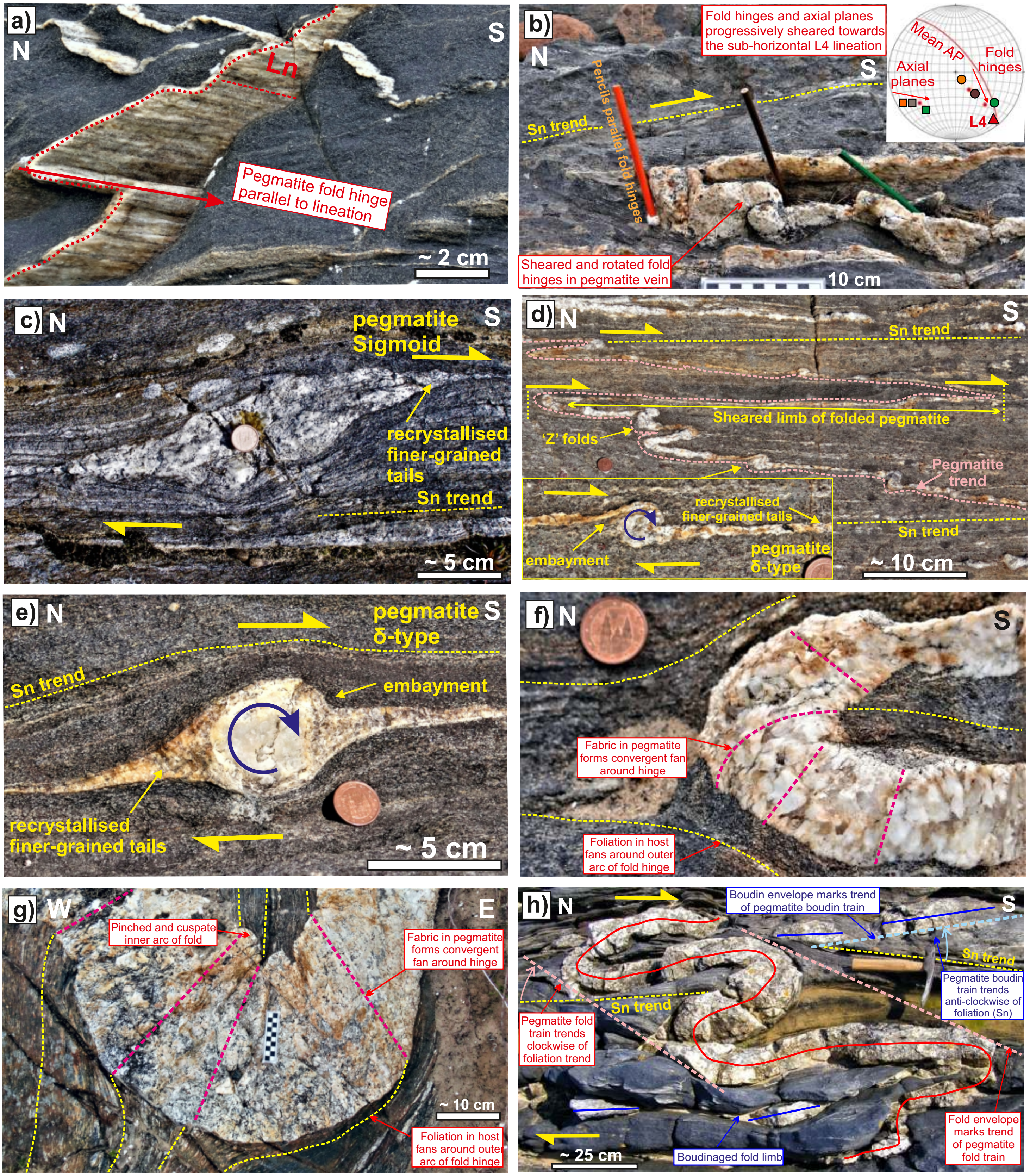
a)
N
S
Ln
Pegmatite fold hinge parallel to lineation
~ 2 cm
b)
N
S
Fold hinges and axial planes progressively sheared towards the sub-horizontal L4 lineation
Mean AP
Axial planes
Fold hinges
L4
Pencils parallel fold hinges
Sn trend
Sheared and rotated fold hinges in pegmatite vein
10 cm
c)
N
S
pegmatite Sigmoid
recrystallised finer-grained tails
Sn trend
~ 5 cm
d)
N
S
Sn trend
Sheared limb of folded pegmatite
'Z' folds
Pegmatite trend
recrystallised finer-grained tails
embayment
pegmatite δ-type
Sn trend
~ 10 cm
e)
N
S
pegmatite δ-type
Sn trend
embayment
recrystallised finer-grained tails
~ 5 cm
f)
N
S
Fabric in pegmatite forms convergent fan around hinge
Foliation in host fans around outer arc of fold hinge
g)
W
E
Pinched and cuspate inner arc of fold
Fabric in pegmatite forms convergent fan around hinge
~ 10 cm
Foliation in host fans around outer arc of fold hinge
h)
N
S
Boudin envelope marks trend of pegmatite boudin train
Sn trend
Sn trend
Pegmatite boudin train trends anti-clockwise of foliation (Sn)
Pegmatite fold train trends clockwise of foliation trend
Fold envelope marks trend of pegmatite fold train
Boudinaged fold limb
~ 25 cm

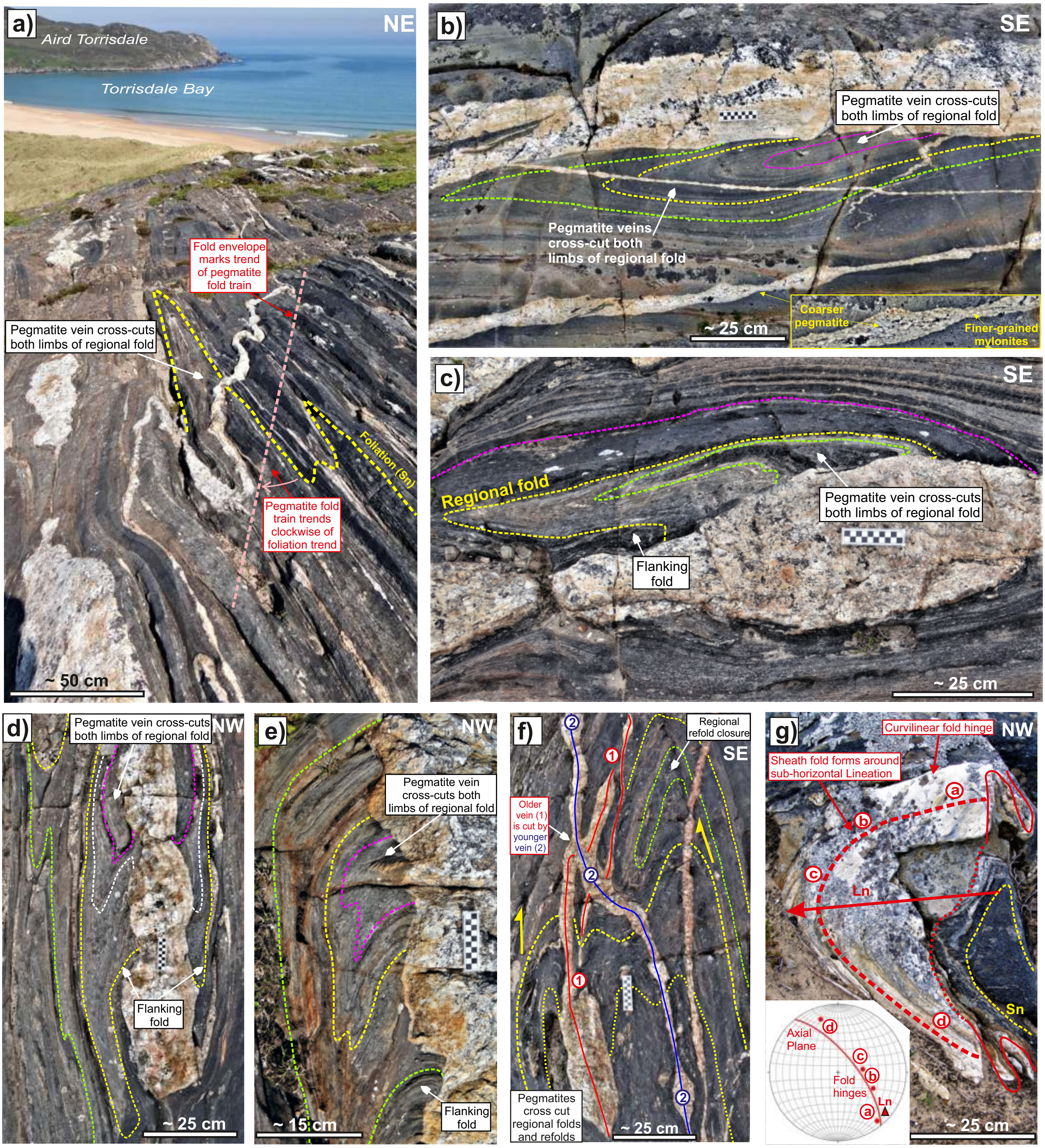
a)
NE
Aird Torrisdale
Torrisdale Bay
Fold envelope marks trend of pegmatite fold train
Pegmatite vein cross-cuts both limbs of regional fold
Foliation (Sn)
Pegmatite fold train trends clockwise of foliation trend
~ 50 cm
b)
SE
Pegmatite vein cross-cuts both limbs of regional fold
Pegmatite veins cross-cut both limbs of regional fold
~ 25 cm
Coarser pegmatite
Finer-grained mylonites
c)
SE
Regional fold
Pegmatite vein cross-cuts both limbs of regional fold
Flanking fold
~ 25 cm
d)
NW
Pegmatite vein cross-cuts both limbs of regional fold
Flanking fold
~ 25 cm
e)
NW
Pegmatite vein cross-cuts both limbs of regional fold
Flanking fold
~ 15 cm
f)
SE
Regional refold closure
Older vein (1) is cut by younger vein (2)
① ② ② ① ②
Pegmatites cross cut regional folds and refolds
~ 25 cm
g)
NW
Curvilinear fold hinge
Sheath fold forms around sub-horizontal Lineation
ⓐ ⓑ ⓒ ⓓ
Ln
Sn
Axial Plane
Fold hinges
ⓓ ⓒ ⓑ ⓐ
Ln
~ 25 cm

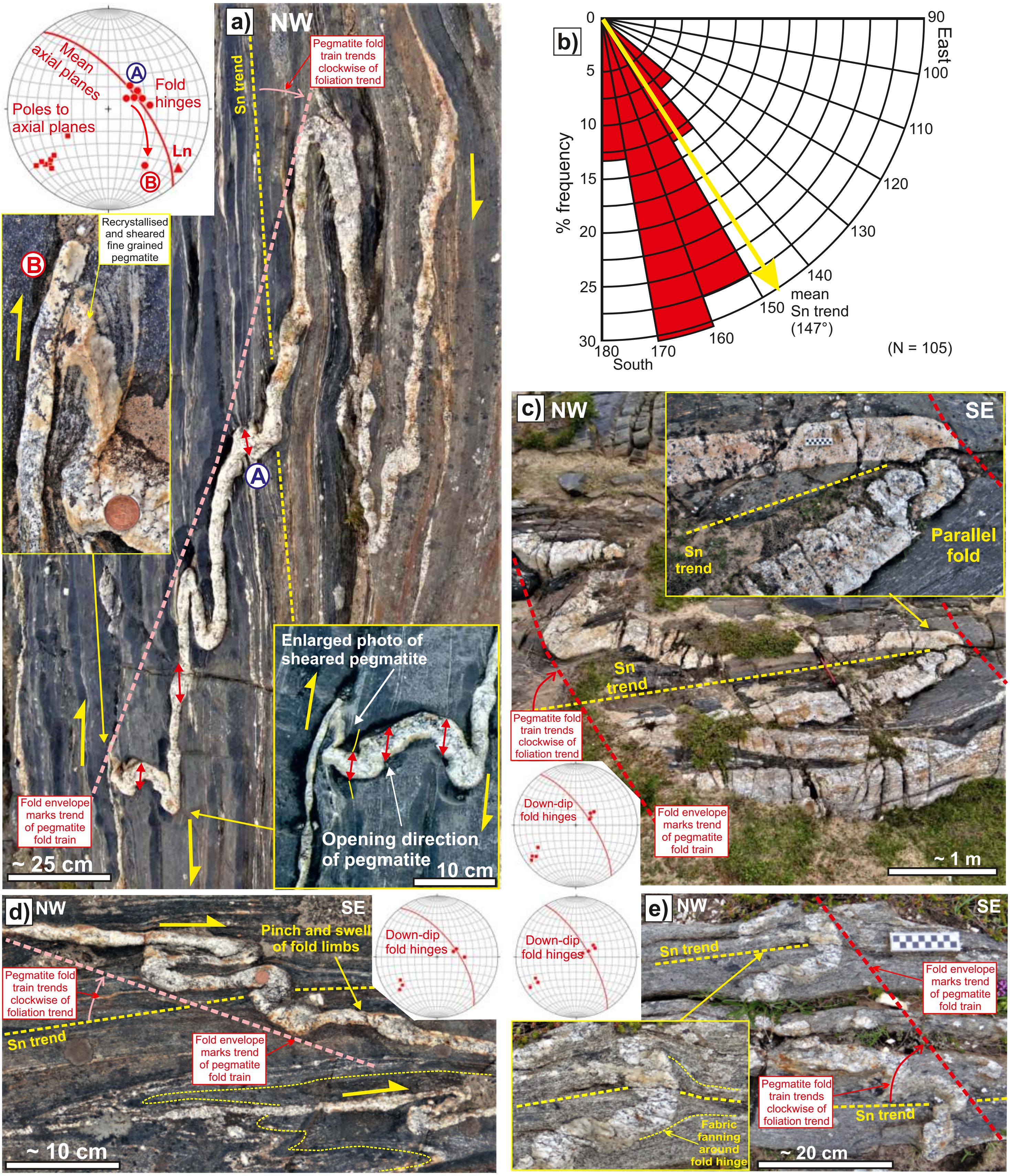

a)
NW
Mean axial planes
A
Fold hinges
Poles to axial planes
Ln
B
Sn trend
Pegmatite fold train trends clockwise of foliation trend
Recrystallised and sheared fine grained pegmatite
B
A
Enlarged photo of sheared pegmatite
Opening direction of pegmatite
10 cm
Fold envelope marks trend of pegmatite fold train
~ 25 cm
b)
0
5
10
15
20
25
30
% frequency
90
East
100
110
120
130
140
150
160
170
180
South
mean Sn trend (147°)
(N = 105)
c) NW
SE
Sn trend
Parallel fold
Sn trend
Pegmatite fold train trends clockwise of foliation trend
Down-dip fold hinges
Fold envelope marks trend of pegmatite fold train
~ 1 m
d) NW
SE
Pinch and swell of fold limbs
Down-dip fold hinges
Pegmatite fold train trends clockwise of foliation trend
Sn trend
Fold envelope marks trend of pegmatite fold train
~ 10 cm
Down-dip fold hinges
e) NW
SE
Sn trend
Fold envelope marks trend of pegmatite fold train
Fabric fanning around fold hinge
Pegmatite fold train trends clockwise of foliation trend
Sn trend
~ 20 cm

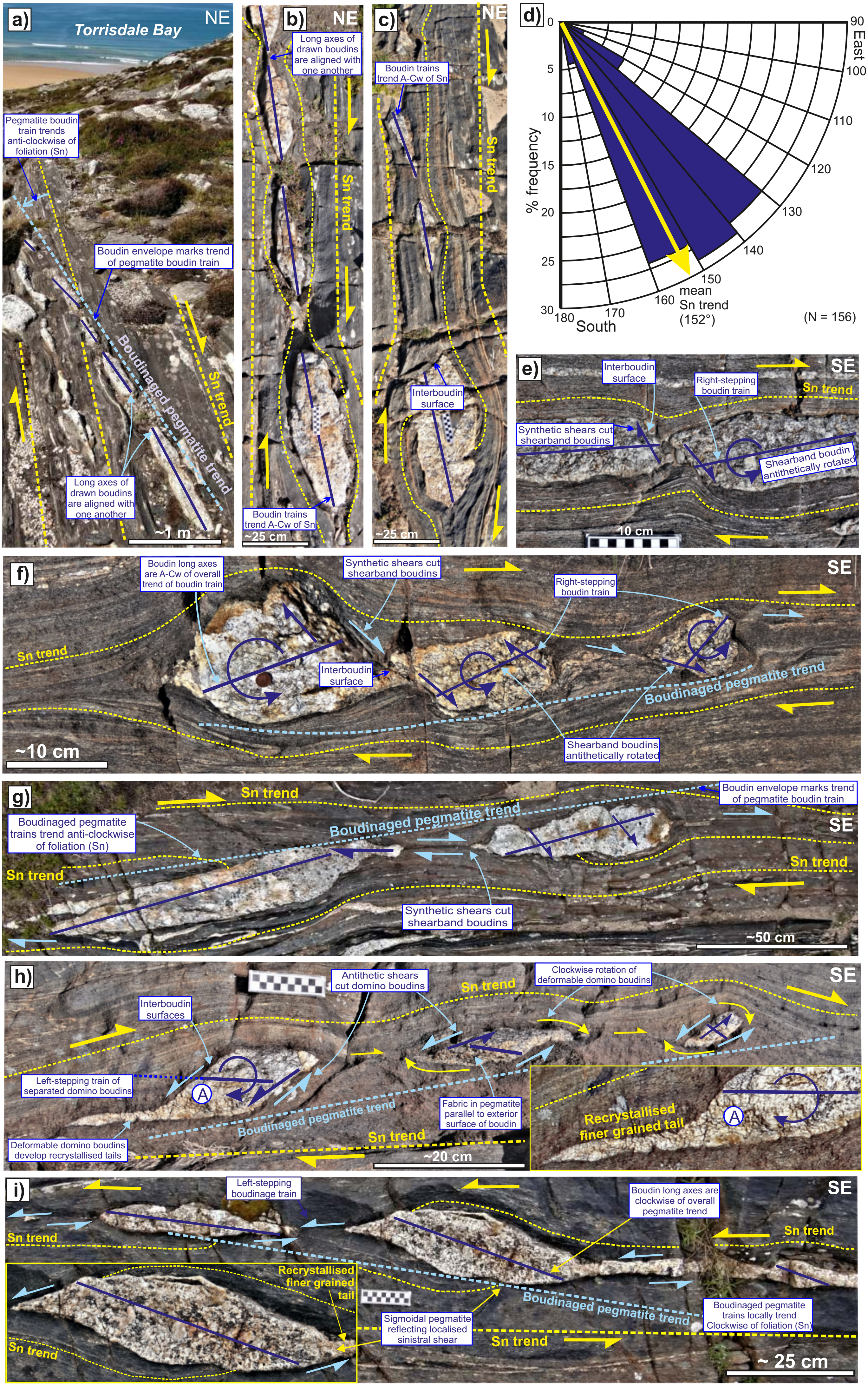
a)
Torrisdale Bay
NE
Pegmatite boudin train trends anti-clockwise of foliation (Sn)
Boudin envelope marks trend of pegmatite boudin train
Boudinaged pegmatite trend
Sn trend
Long axes of drawn boudins are aligned with one another
~1 m
b)
NE
Long axes of drawn boudins are aligned with one another
Sn trend
Boudin trains trend A-Cw of Sn
~25 cm
c)
NE
Boudin trains trend A-Cw of Sn
Sn trend
Interboudin surface
~25 cm
d)
0
5
10
15
20
25
30
% frequency
90
East
100
110
120
130
140
150
160
170
180
South
mean Sn trend (152°)
(N = 156)
e)
SE
Interboudin surface
Right-stepping boudin train
Sn trend
Synthetic shears cut shearband boudins
Shearband boudin antithetically rotated
10 cm
f)
SE
Boudin long axes are A-Cw of overall trend of boudin train
Synthetic shears cut shearband boudins
Right-stepping boudin train
Sn trend
Interboudin surface
Boudinaged pegmatite trend
Shearband boudins antithetically rotated
~10 cm
g)
Sn trend
Boudin envelope marks trend of pegmatite boudin train
SE
Boudinaged pegmatite trains trend anti-clockwise of foliation (Sn)
Boudinaged pegmatite trend
Sn trend
Sn trend
Synthetic shears cut shearband boudins
~50 cm
h)
Antithetic shears cut domino boudins
Clockwise rotation of deformable domino boudins
SE
Sn trend
Interboudin surfaces
Left-stepping train of separated domino boudins
A
Boudinaged pegmatite trend
Fabric in pegmatite parallel to exterior surface of boudin
Recrystallised finer grained tail
A
Sn trend
Deformable domino boudins develop recrystallised tails
~20 cm
i)
Left-stepping boudinage train
Boudin long axes are clockwise of overall pegmatite trend
SE
Sn trend
Sn trend
Recrystallised finer grained tail
Sn trend
Sigmoidal pegmatite reflecting localised sinistral shear
Boudinaged pegmatite trend
Boudinaged pegmatite trains locally trend Clockwise of foliation (Sn)
Sn trend
~ 25 cm

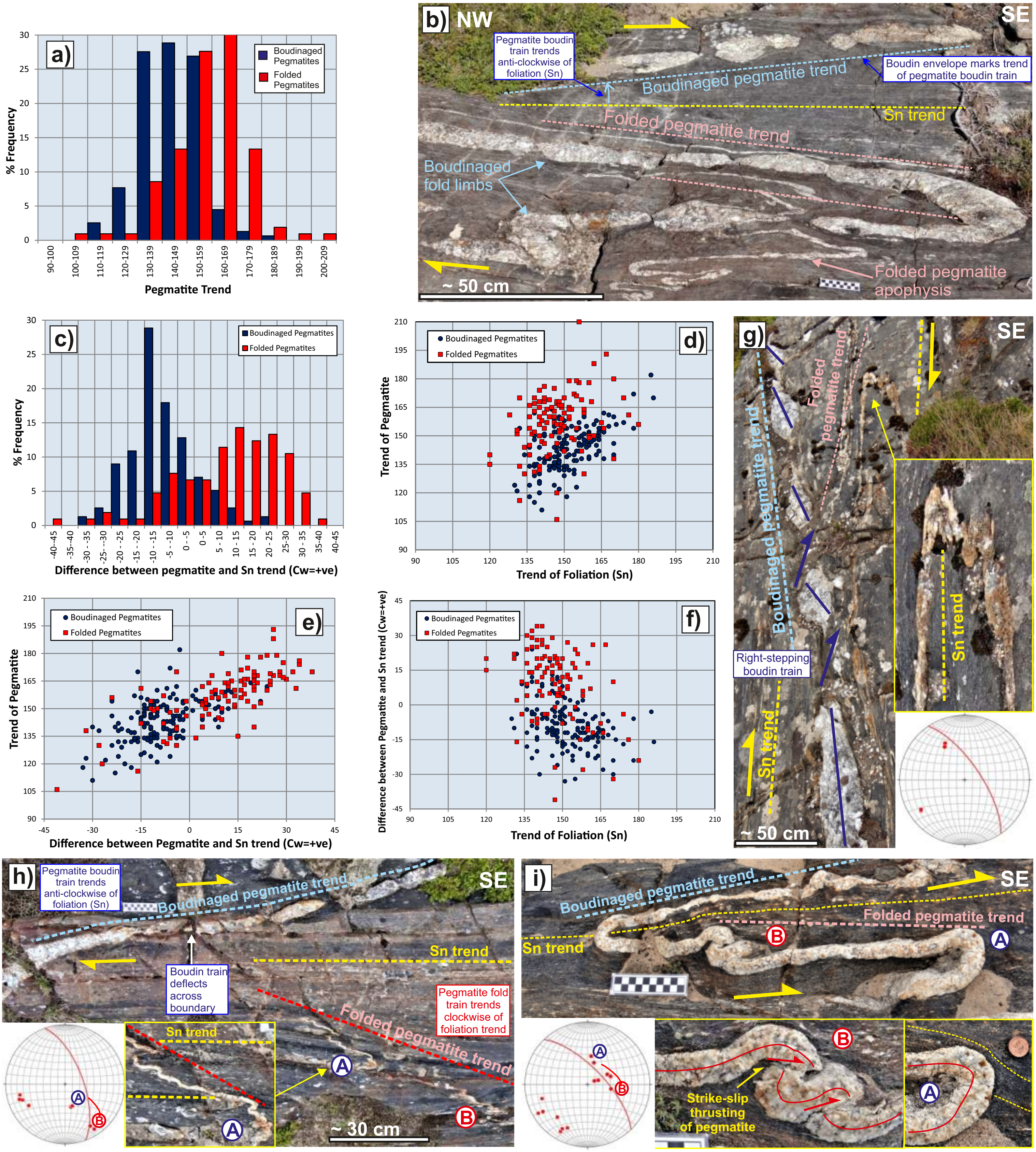
a)
% Frequency
Pegmatite Trend
Boudinaged Pegmatites
Folded Pegmatites
90-100
100-109
110-119
120-129
130-139
140-149
150-159
160-169
170-179
180-189
190-199
200-209
b) NW
SE
Pegmatite boudin train trends anti-clockwise of foliation (Sn)
Boudin envelope marks trend of pegmatite boudin train
Boudinaged pegmatite trend
Sn trend
Folded pegmatite trend
Boudinaged fold limbs
Folded pegmatite apophysis
~ 50 cm
c)
% Frequency
Difference between pegmatite and Sn trend (Cw=+ve)
Boudinaged Pegmatites
Folded Pegmatites
-40-45
-35--40
-30 - -35
-25 - -30
-20 - -25
-15 - -20
-10 - -15
-5 - -10
0 - -5
0 - 5
5 - 10
10 - 15
15 - 20
20 - 25
25-30
30 - 35
35-40
40-45
d)
Trend of Pegmatite
Trend of Foliation (Sn)
Boudinaged Pegmatites
Folded Pegmatites
e)
Trend of Pegmatite
Difference between Pegmatite and Sn trend (Cw=+ve)
Boudinaged Pegmatites
Folded Pegmatites
f)
Difference between Pegmatite and Sn trend (Cw=+ve)
Trend of Foliation (Sn)
Boudinaged Pegmatites
Folded Pegmatites
g)
SE
Boudinaged pegmatite trend
Folded pegmatite trend
Right-stepping boudin train
Sn trend
Sn trend
~ 50 cm
h)
SE
Pegmatite boudin train trends anti-clockwise of foliation (Sn)
Boudinaged pegmatite trend
Boudin train deflects across boundary
Sn trend
Pegmatite fold train trends clockwise of foliation trend
Folded pegmatite trend
Sn trend
A
A
B
B
~ 30 cm
i)
SE
Boudinaged pegmatite trend
Folded pegmatite trend
Sn trend
A
B
A
B
B
A
Strike-slip thrusting of pegmatite

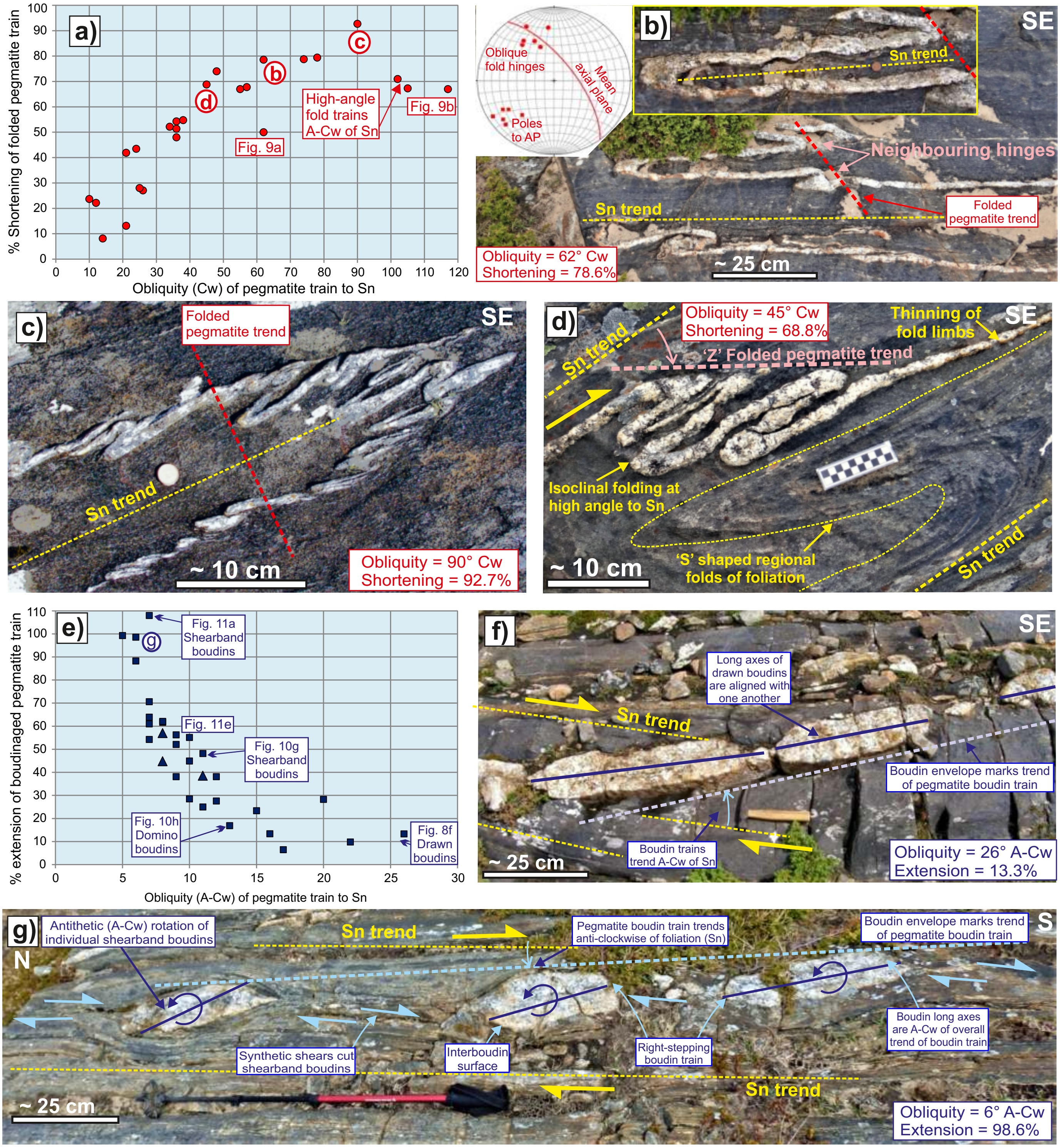
a)
% Shortening of folded pegmatite train
Obliquity (Cw) of pegmatite train to Sn
0
10
20
30
40
50
60
70
80
90
100
110
120
b
c
d
Fig. 9a
Fig. 9b
High-angle fold trains A-Cw of Sn
b)
SE
Oblique fold hinges
Mean axial plane
Poles to AP
Sn trend
Neighbouring hinges
Folded pegmatite trend
Obliquity = 62° Cw
Shortening = 78.6%
~ 25 cm
c)
SE
Folded pegmatite trend
Sn trend
~ 10 cm
Obliquity = 90° Cw
Shortening = 92.7%
d)
SE
Sn trend
Obliquity = 45° Cw
Shortening = 68.8%
Thinning of fold limbs
'Z' Folded pegmatite trend
Isoclinal folding at high angle to Sn
'S' shaped regional folds of foliation
~ 10 cm
e)
% extension of boudinaged pegmatite train
Obliquity (A-Cw) of pegmatite train to Sn
0
5
10
15
20
25
30
110
100
90
80
70
60
50
40
30
20
10
0
g
Fig. 11a Shearband boudins
Fig. 11e
Fig. 10g Shearband boudins
Fig. 10h Domino boudins
Fig. 8f Drawn boudins
f)
SE
Long axes of drawn boudins are aligned with one another
Sn trend
Boudin envelope marks trend of pegmatite boudin train
Boudin trains trend A-Cw of Sn
~ 25 cm
Obliquity = 26° A-Cw
Extension = 13.3%
g)
N
S
Antithetic (A-Cw) rotation of individual shearband boudins
Sn trend
Pegmatite boudin train trends anti-clockwise of foliation (Sn)
Boudin envelope marks trend of pegmatite boudin train
Synthetic shears cut shearband boudins
Interboudin surface
Right-stepping boudin train
Boudin long axes are A-Cw of overall trend of boudin train
~ 25 cm
Obliquity = 6° A-Cw
Extension = 98.6%

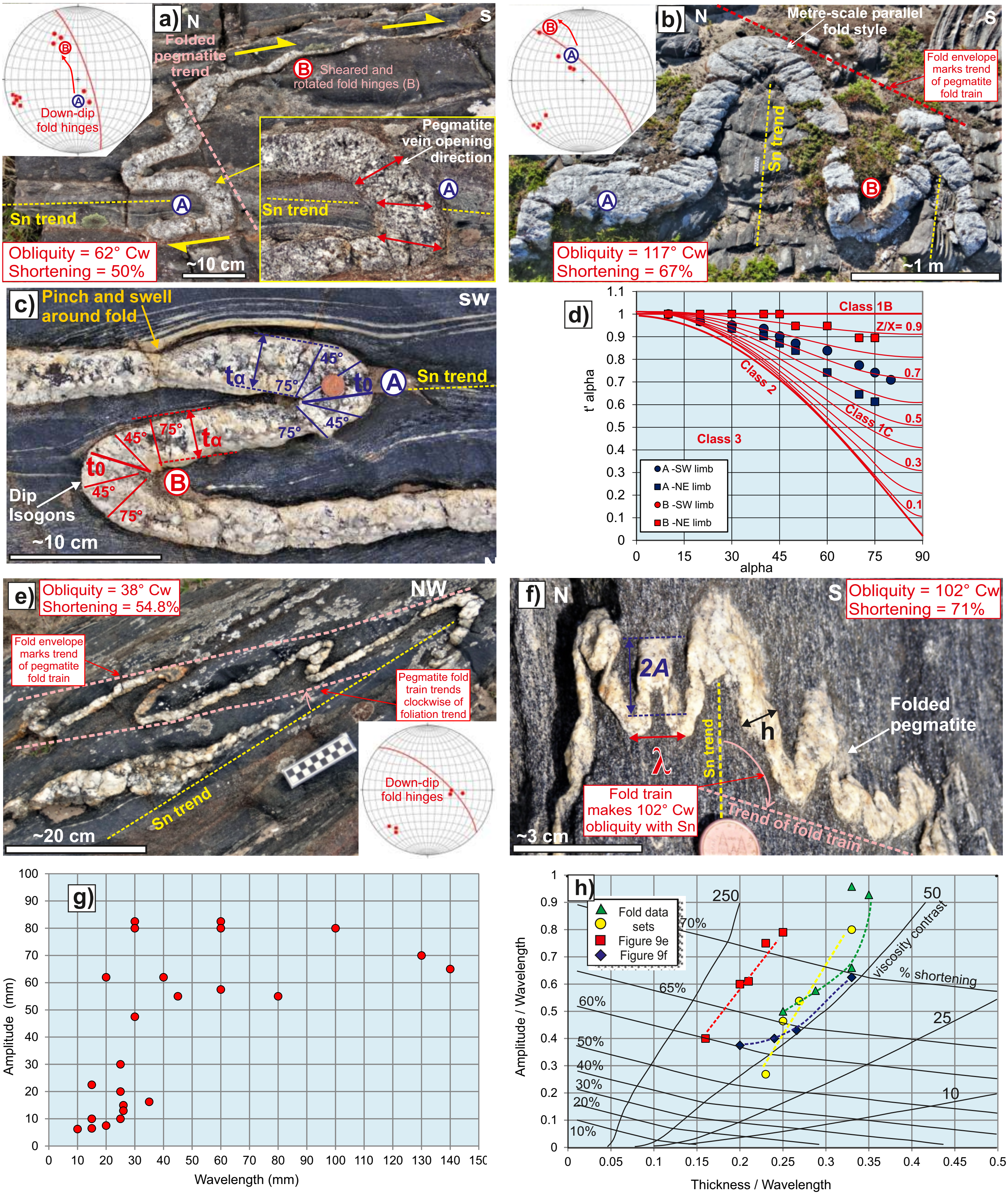

a) N
S
Folded pegmatite trend
B Sheared and rotated fold hinges (B)
Down-dip fold hinges
Pegmatite vein opening direction
Sn trend
A
B
Obliquity = 62° Cw
Shortening = 50%
~10 cm
b) N
S
Metre-scale parallel fold style
Fold envelope marks trend of pegmatite fold train
Sn trend
Obliquity = 117° Cw
Shortening = 67%
~1 m
c) Pinch and swell around fold
SW
Sn trend
tα
t0
45°
75°
Dip Isogons
~10 cm
d)
t' alpha
alpha
Class 1B
Z/X= 0.9
0.7
0.5
0.3
0.1
Class 2
Class 1C
Class 3
A -SW limb
A -NE limb
B -SW limb
B -NE limb
e) Obliquity = 38° Cw
Shortening = 54.8%
NW
Fold envelope marks trend of pegmatite fold train
Pegmatite fold train trends clockwise of foliation trend
Sn trend
Down-dip fold hinges
~20 cm
f) N
S
Obliquity = 102° Cw
Shortening = 71%
2A
λ
h
Sn trend
Folded pegmatite
Fold train makes 102° Cw obliquity with Sn
Trend of fold train
~3 cm
g)
Amplitude (mm)
Wavelength (mm)
h)
Fold data sets
Figure 9e
Figure 9f
Amplitude / Wavelength
Thickness / Wavelength
250
50
25
10
viscosity contrast
% shortening
70%
65%
60%
50%
40%
30%
20%
10%

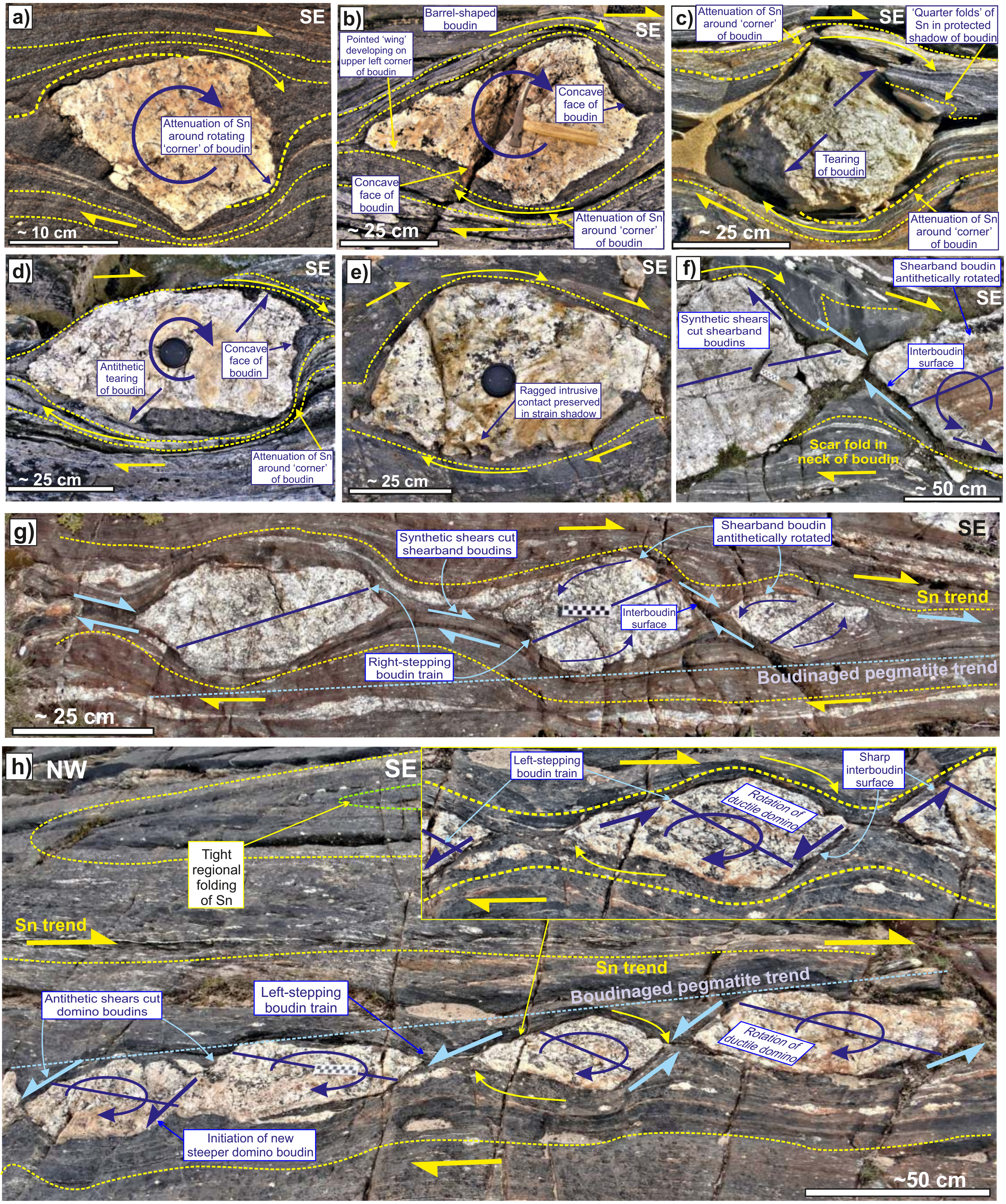
a)
SE
Attenuation of Sn around rotating 'corner' of boudin
~ 10 cm
b)
Barrel-shaped boudin
SE
Pointed 'wing' developing on upper left corner of boudin
Concave face of boudin
Concave face of boudin
Attenuation of Sn around 'corner' of boudin
~ 25 cm
c)
Attenuation of Sn around 'corner' of boudin
SE
'Quarter folds' of Sn in protected shadow of boudin
Tearing of boudin
Attenuation of Sn around 'corner' of boudin
~ 25 cm
d)
SE
Antithetic tearing of boudin
Concave face of boudin
Attenuation of Sn around 'corner' of boudin
~ 25 cm
e)
SE
Ragged intrusive contact preserved in strain shadow
~ 25 cm
f)
Shearband boudin antithetically rotated
SE
Synthetic shears cut shearband boudins
Interboudin surface
Scar fold in neck of boudin
~ 50 cm
g)
SE
Synthetic shears cut shearband boudins
Shearband boudin antithetically rotated
Interboudin surface
Sn trend
Right-stepping boudin train
Boudinaged pegmatite trend
~ 25 cm
h)
NW
SE
Tight regional folding of Sn
Left-stepping boudin train
Rotation of ductile domino
Sharp interboudin surface
Sn trend
Sn trend
Boudinaged pegmatite trend
Antithetic shears cut domino boudins
Left-stepping boudin train
Rotation of ductile domino
Initiation of new steeper domino boudin
~50 cm

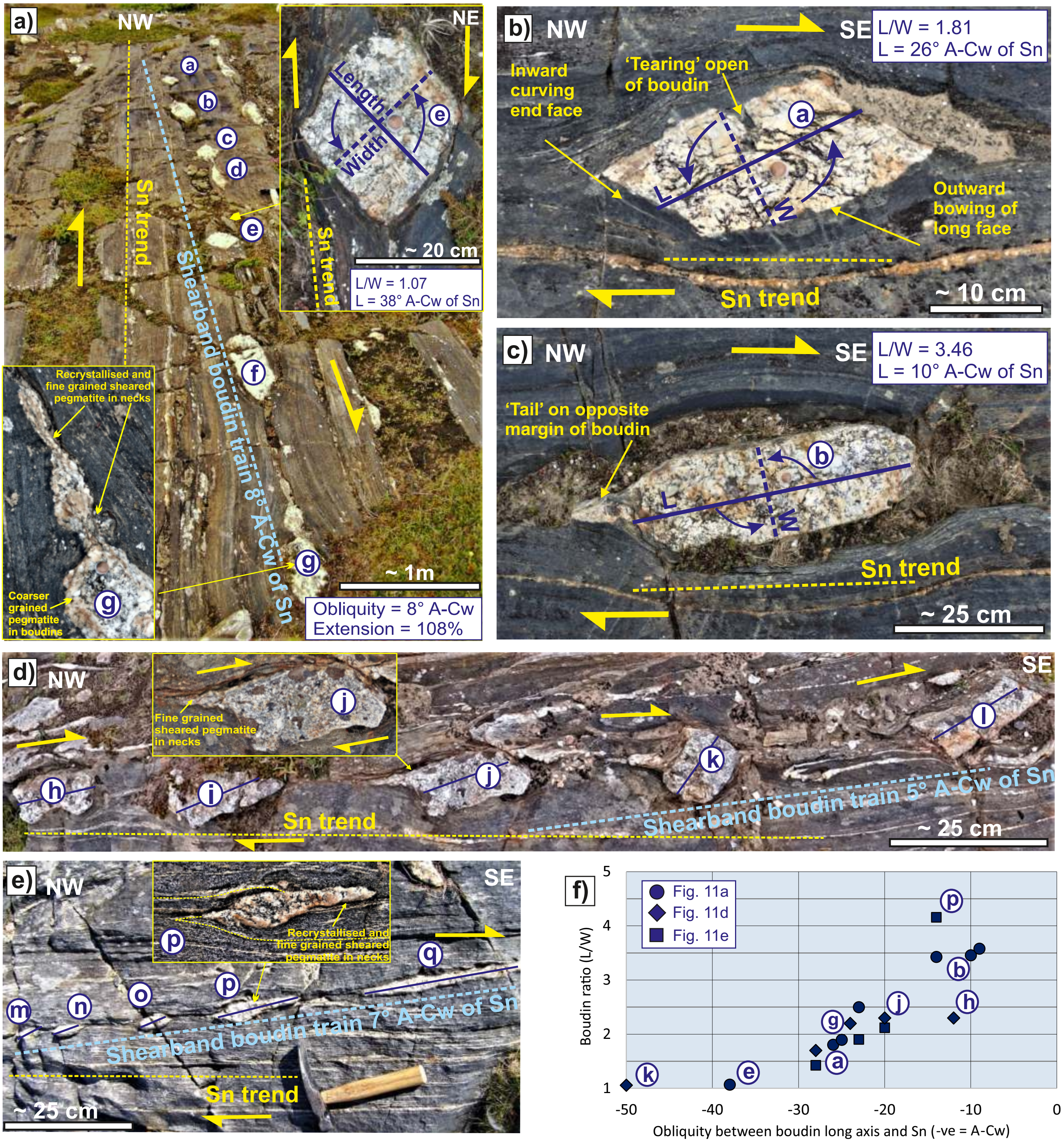a)
NW
NE
a
b
c
d
e
f
g
Sn trend
Shearband boudin train 8° A-Cw of Sn
Length
Width
~ 20 cm
L/W = 1.07
L = 38° A-Cw of Sn
Recrystallised and fine grained sheared pegmatite in necks
Coarser grained pegmatite in boudins
~ 1m
Obliquity = 8° A-Cw
Extension = 108%
b)
NW
SE
L/W = 1.81
L = 26° A-Cw of Sn
Inward curving end face
'Tearing' open of boudin
Outward bowing of long face
L
W
Sn trend
~ 10 cm
c)
NW
SE
L/W = 3.46
L = 10° A-Cw of Sn
'Tail' on opposite margin of boudin
L
W
Sn trend
~ 25 cm
d)
NW
SE
Fine grained sheared pegmatite in necks
h
i
j
k
l
Sn trend
Shearband boudin train 5° A-Cw of Sn
~ 25 cm
e)
NW
SE
Recrystallised and fine grained sheared pegmatite in necks
m
n
o
p
q
Shearband boudin train 7° A-Cw of Sn
Sn trend
~ 25 cm
f)
Fig. 11a
Fig. 11d
Fig. 11e
Boudin ratio (L/W)
Obliquity between boudin long axis and Sn (-ve = A-Cw)
5
4
3
2
1
-50
-40
-30
-20
-10
0

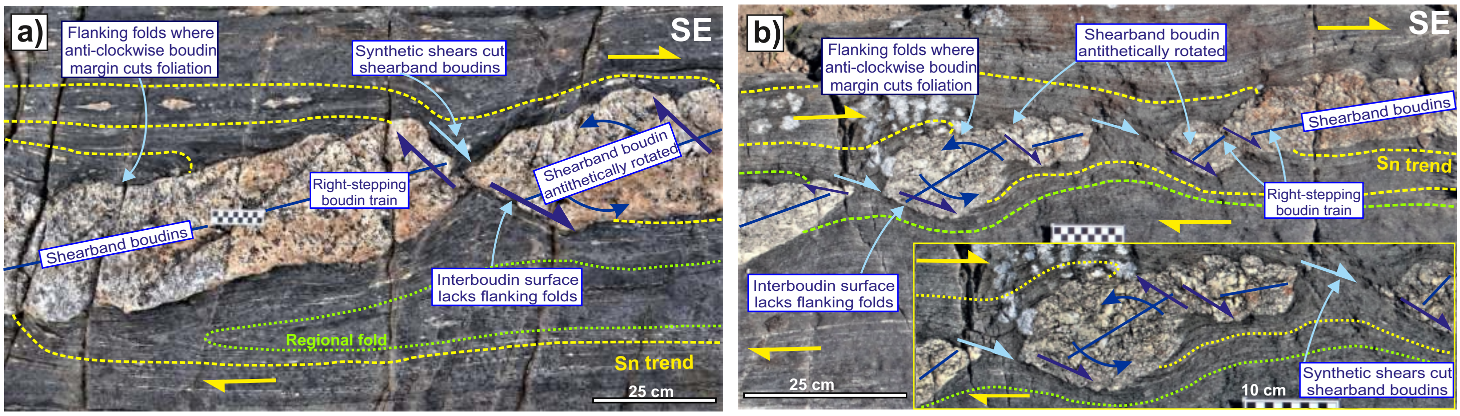
a)
SE
Flanking folds where anti-clockwise boudin margin cuts foliation
Synthetic shears cut shearband boudins
Right-stepping boudin train
Shearband boudin antithetically rotated
Shearband boudins
Interboudin surface lacks flanking folds
Regional fold
Sn trend
25 cm
b)
SE
Flanking folds where anti-clockwise boudin margin cuts foliation
Shearband boudin antithetically rotated
Shearband boudins
Sn trend
Right-stepping boudin train
Interboudin surface lacks flanking folds
25 cm
10 cm
Synthetic shears cut shearband boudins

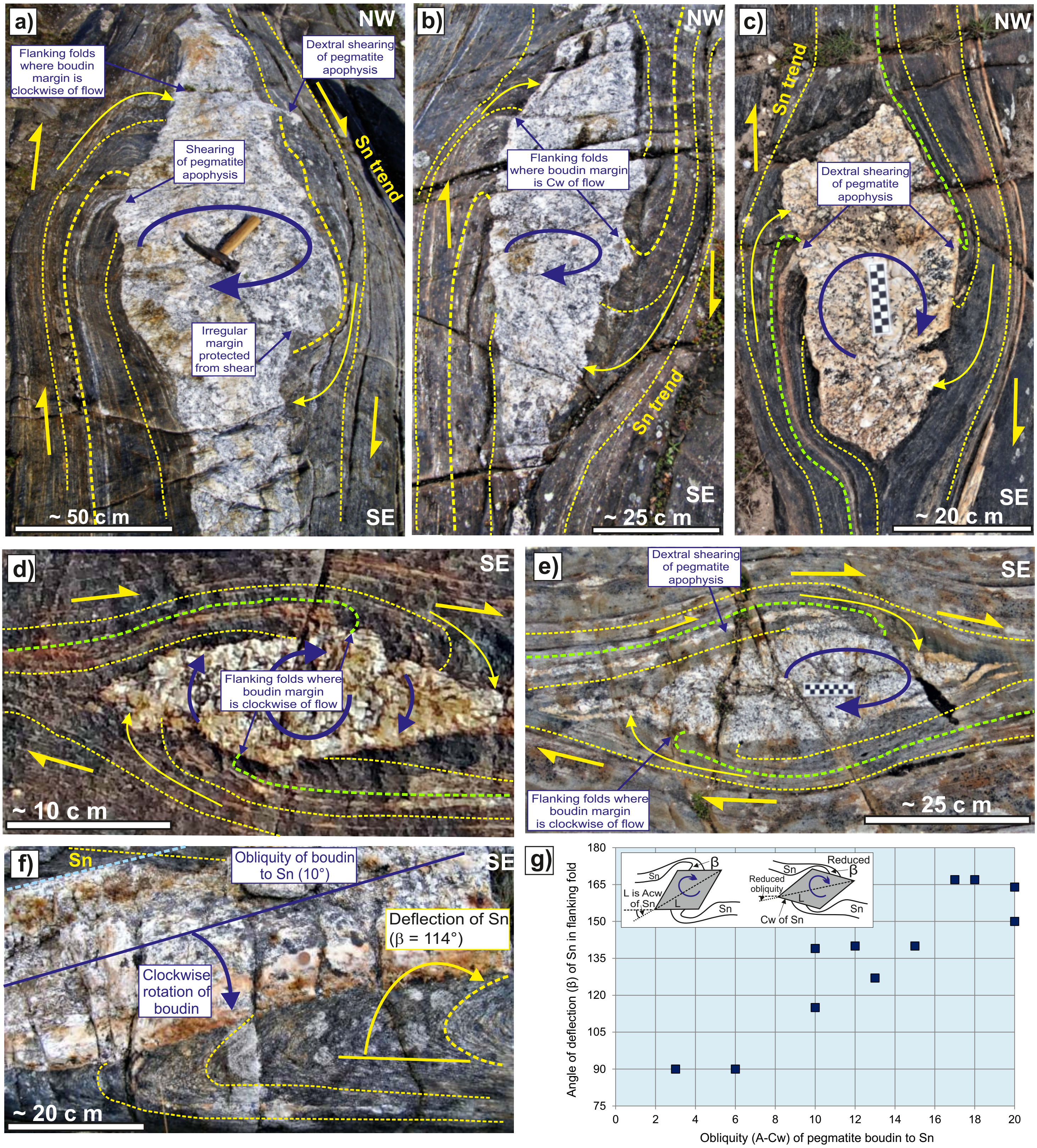
a)
NW
Flanking folds where boudin margin is clockwise of flow
Dextral shearing of pegmatite apophysis
Shearing of pegmatite apophysis
Sn trend
Irregular margin protected from shear
~ 50 c m
SE
b)
NW
Flanking folds where boudin margin is Cw of flow
Sn trend
SE
~ 25 c m
c)
NW
Sn trend
Dextral shearing of pegmatite apophysis
SE
~ 20 c m
d)
SE
Flanking folds where boudin margin is clockwise of flow
~ 10 c m
e)
SE
Dextral shearing of pegmatite apophysis
Flanking folds where boudin margin is clockwise of flow
~ 25 c m
f)
Sn
Obliquity of boudin to Sn (10°)
SE
Deflection of Sn (β = 114°)
Clockwise rotation of boudin
~ 20 c m
g)
β
Sn
L is Acw of Sn
L
Sn
Reduced β
Sn
Reduced obliquity
L
Cw of Sn
Sn
Angle of deflection (β) of Sn in flanking fold
180
165
150
135
120
105
90
75
0
2
4
6
8
10
12
14
16
18
20
Obliquity (A-Cw) of pegmatite boudin to Sn

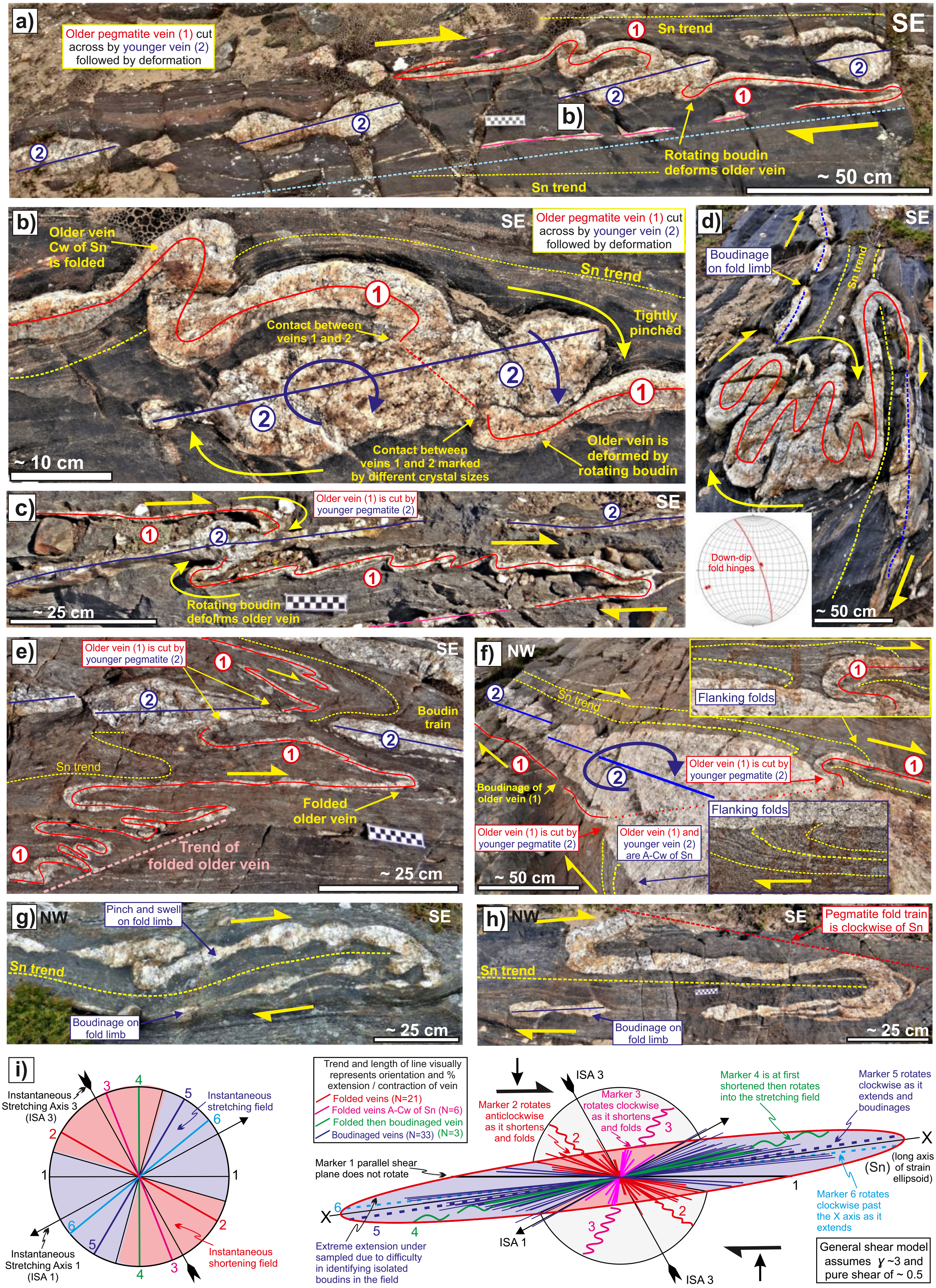
a)
Older pegmatite vein (1) cut across by younger vein (2) followed by deformation
SE
Sn trend
b)
Rotating boudin deforms older vein
~ 50 cm
b)
Older vein Cw of Sn is folded
SE
Older pegmatite vein (1) cut across by younger vein (2) followed by deformation
Sn trend
Tightly pinched
Contact between veins 1 and 2
Contact between veins 1 and 2 marked by different crystal sizes
Older vein is deformed by rotating boudin
~ 10 cm
c)
Older vein (1) is cut by younger pegmatite (2)
SE
Rotating boudin defolrms older vein
~ 25 cm
d)
SE
Boudinage on fold limb
Sn trend
Down-dip fold hinges
~ 50 cm
e)
Older vein (1) is cut by younger pegmatite (2)
SE
Boudin train
Sn trend
Folded older vein
Trend of folded older vein
~ 25 cm
f)
NW
Sn trend
Flanking folds
Older vein (1) is cut by younger pegmatite (2)
Boudinage of older vein (1)
Older vein (1) is cut by younger pegmatite (2)
Older vein (1) and younger vein (2) are A-Cw of Sn
Flanking folds
~ 50 cm
g)
NW
SE
Pinch and swell on fold limb
Sn trend
Boudinage on fold limb
~ 25 cm
h)
NW
SE
Pegmatite fold train is clockwise of Sn
Sn trend
Boudinage on fold limb
~ 25 cm
i)
Instantaneous Stretching Axis 3 (ISA 3)
Instantaneous stretching field
Instantaneous Stretching Axis 1 (ISA 1)
Instantaneous shortening field
1
2
3
4
5
6
Trend and length of line visually represents orientation and % extension / contraction of vein
Folded veins (N=21)
Folded veins A-Cw of Sn (N=6)
Folded then boudinaged vein (N=3)
Boudinaged veins (N=33)
ISA 3
Marker 2 rotates anticlockwise as it shortens and folds
Marker 3 rotates clockwise as it shortens and folds
Marker 4 is at first shortened then rotates into the stretching field
Marker 5 rotates clockwise as it extends and boudinages
X
(long axis of strain ellipsoid)
(Sn)
Marker 1 parallel shear plane does not rotate
Marker 6 rotates clockwise past the X axis as it extends
Extreme extension under sampled due to difficulty in identifying isolated boudins in the field
ISA 1
ISA 3
General shear model assumes γ ~3 and pure shear of ~ 0.5

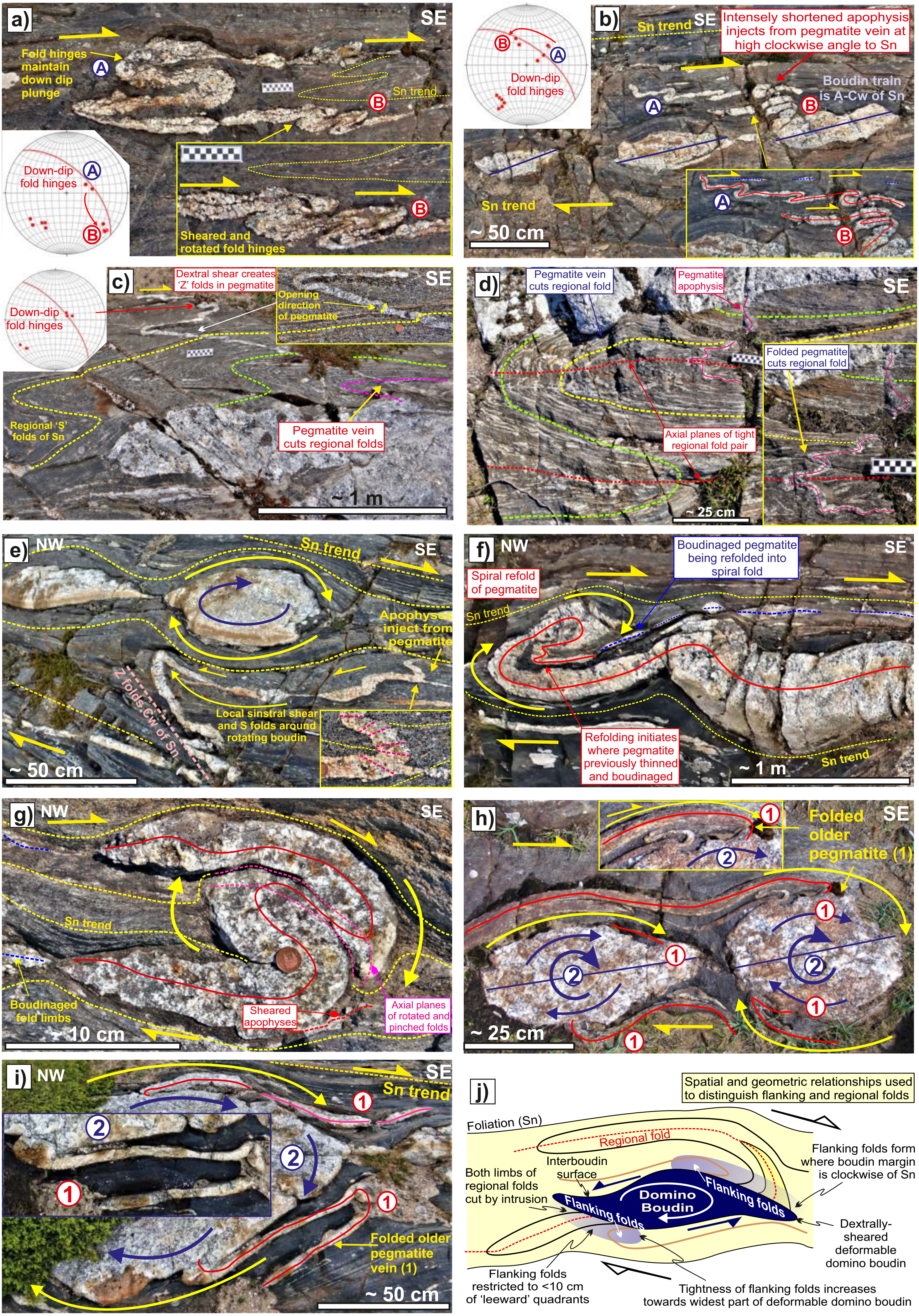

a)
SE
Fold hinges maintain down dip plunge
A
B
Sn trend
Down-dip fold hinges
Sheared and rotated fold hinges
b)
Sn trend
SE
Intensely shortened apophysis injects from pegmatite vein at high clockwise angle to Sn
Down-dip fold hinges
Boudin train is A-Cw of Sn
Sn trend
~ 50 cm
c)
Dextral shear creates 'Z' folds in pegmatite
SE
Opening direction of pegmatite
Down-dip fold hinges
Regional 'S' folds of Sn
Pegmatite vein cuts regional folds
~ 1 m
d)
Pegmatite vein cuts regional fold
Pegmatite apophysis
SE
Folded pegmatite cuts regional fold
Axial planes of tight regional fold pair
~ 25 cm
e)
NW
Sn trend
SE
Apophyses inject from pegmatite
Z folds Cw of Sn
Local sinstral shear and S folds around rotating boudin
~ 50 cm
f)
NW
SE
Boudinaged pegmatite being refolded into spiral fold
Spiral refold of pegmatite
Sn trend
Refolding initiates where pegmatite previously thinned and boudinaged
~ 1 m
Sn trend
g)
NW
SE
Sn trend
Boudinaged fold limbs
Sheared apophyses
Axial planes of rotated and pinched folds
~ 10 cm
h)
SE
Folded older pegmatite (1)
1
2
~ 25 cm
i)
NW
SE
Sn trend
1
2
Folded older pegmatite vein (1)
~ 50 cm
j)
Spatial and geometric relationships used to distinguish flanking and regional folds
Foliation (Sn)
Regional fold
Interboudin surface
Both limbs of regional folds cut by intrusion
Flanking folds
Domino Boudin
Flanking folds
Flanking folds form where boudin margin is clockwise of Sn
Dextrally-sheared deformable domino boudin
Flanking folds restricted to <10 cm of 'leeward' quadrants
Tightness of flanking folds increases towards widest part of deformable domino boudin

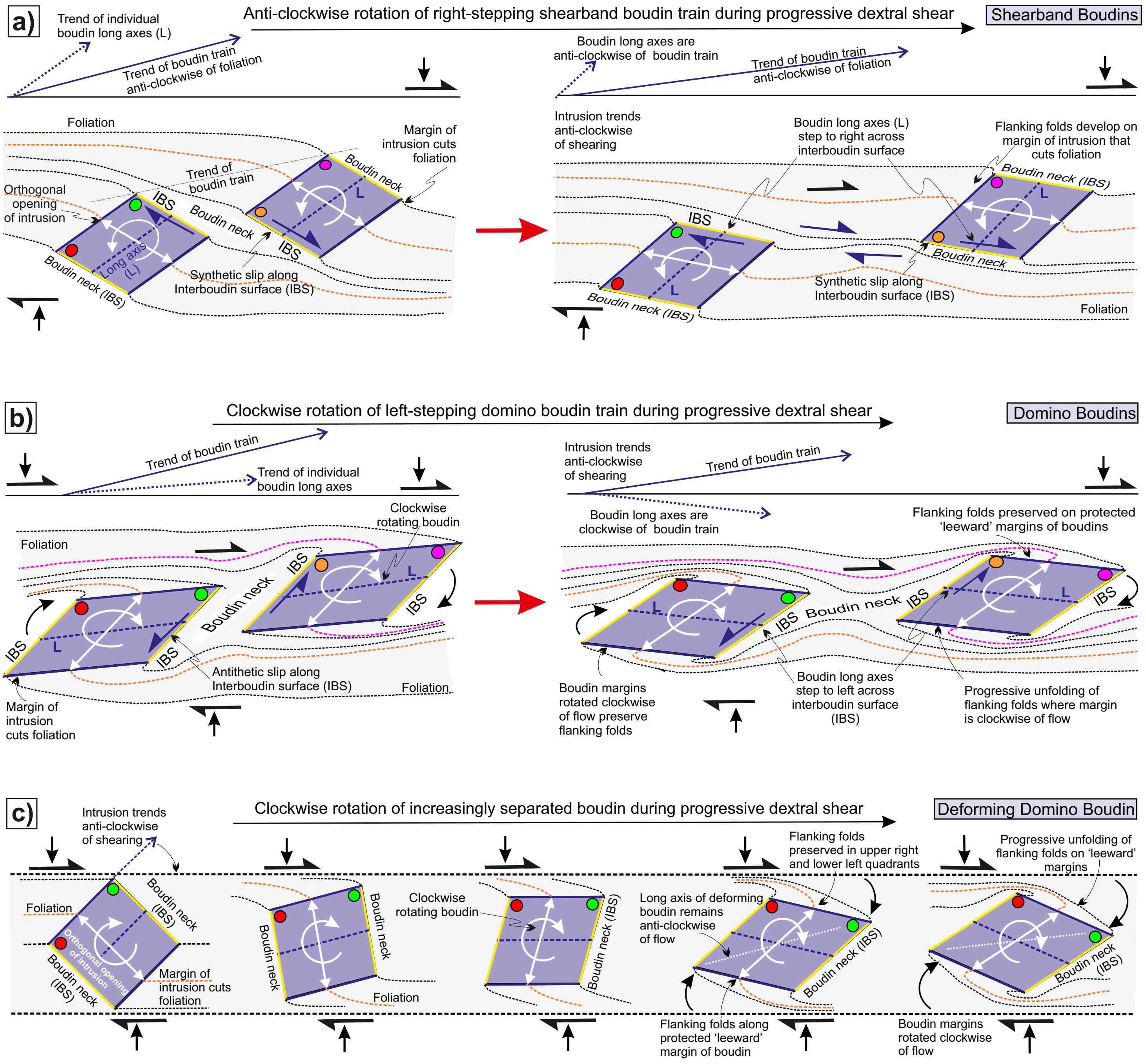
a)
Anti-clockwise rotation of right-stepping shearband boudin train during progressive dextral shear
Shearband Boudins
Trend of individual boudin long axes (L)
Trend of boudin train anti-clockwise of foliation
Foliation
Margin of intrusion cuts foliation
Trend of boudin train
Orthogonal opening of intrusion
IBS
Boudin neck
Boudin neck
IBS
Long axis (L)
L
Boudin neck (IBS)
Synthetic slip along Interboudin surface (IBS)
Boudin long axes are anti-clockwise of boudin train
Trend of boudin train anti-clockwise of foliation
Intrusion trends anti-clockwise of shearing
Boudin long axes (L) step to right across interboudin surface
Flanking folds develop on margin of intrusion that cuts foliation
Boudin neck (IBS)
IBS
L
Boudin neck
L
Synthetic slip along Interboudin surface (IBS)
Boudin neck (IBS)
Foliation
b)
Clockwise rotation of left-stepping domino boudin train during progressive dextral shear
Domino Boudins
Trend of boudin train
Trend of individual boudin long axes
Clockwise rotating boudin
Foliation
IBS
Boudin neck
L
IBS
L
IBS
IBS
Antithetic slip along Interboudin surface (IBS)
Foliation
Margin of intrusion cuts foliation
Intrusion trends anti-clockwise of shearing
Trend of boudin train
Boudin long axes are clockwise of boudin train
Flanking folds preserved on protected 'leeward' margins of boudins
L
IBS
Boudin neck
IBS
L
IBS
Boudin margins rotated clockwise of flow preserve flanking folds
Boudin long axes step to left across interboudin surface (IBS)
Progressive unfolding of flanking folds where margin is clockwise of flow
c)
Clockwise rotation of increasingly separated boudin during progressive dextral shear
Deforming Domino Boudin
Intrusion trends anti-clockwise of shearing
Foliation
Boudin neck (IBS)
Orthogonal opening of intrusion
Boudin neck (IBS)
Margin of intrusion cuts foliation
Boudin neck
Boudin neck
Foliation
Clockwise rotating boudin
Boudin neck (IBS)
Long axis of deforming boudin remains anti-clockwise of flow
Flanking folds preserved in upper right and lower left quadrants
Boudin neck (IBS)
Flanking folds along protected 'leeward' margin of boudin
Progressive unfolding of flanking folds on 'leeward' margins
Boudin neck (IBS)
Boudin margins rotated clockwise of flow

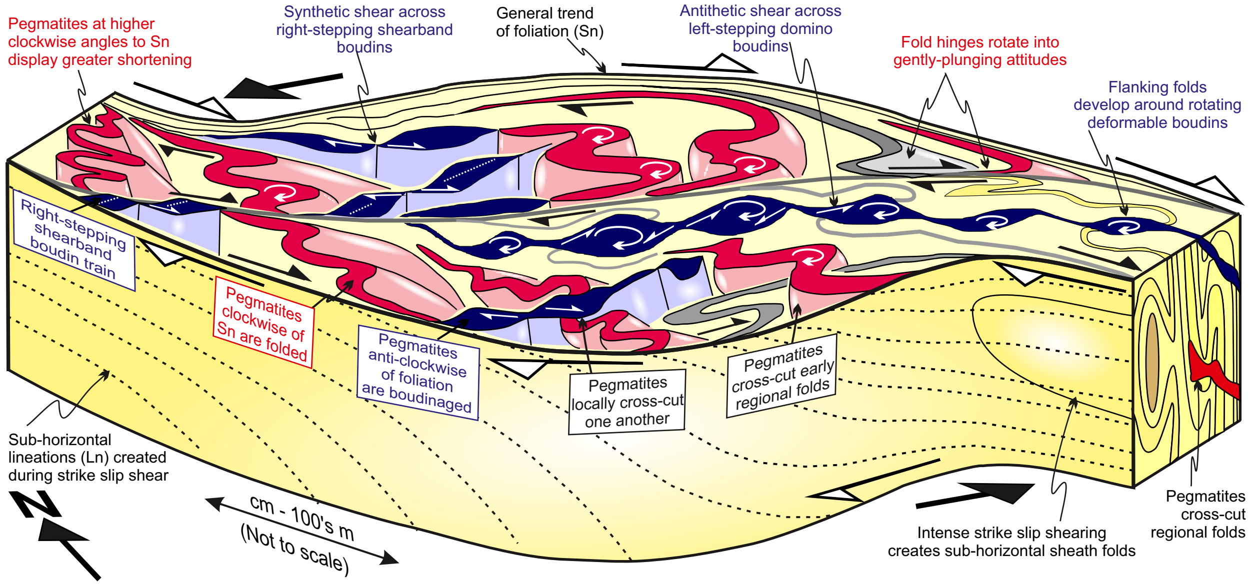
Pegmatites at higher clockwise angles to Sn display greater shortening
Synthetic shear across right-stepping shearband boudins
General trend of foliation (Sn)
Antithetic shear across left-stepping domino boudins
Fold hinges rotate into gently-plunging attitudes
Flanking folds develop around rotating deformable boudins
Right-stepping shearband boudin train
Pegmatites clockwise of Sn are folded
Pegmatites anti-clockwise of foliation are boudinaged
Pegmatites locally cross-cut one another
Pegmatites cross-cut early regional folds
Sub-horizontal lineations (Ln) created during strike slip shear
N
cm - 100's m
(Not to scale)
Intense strike slip shearing creates sub-horizontal sheath folds
Pegmatites cross-cut regional folds